NUREG/CR-4667, Vol. 14
ANL-92/30

Environmentally Assisted Cracking in Light Water Reactors

Semiannual Report
October 1991–March 1992

Prepared by
H. M. Chung, T. F. Kassner, S. Majumdar, J. Y. Park,
A. Purohit, W. E. Ruther, J. E. Sanecki, W. J. Shack

Argonne National Laboratory

Prepared for
U.S. Nuclear Regulatory Commission

AVAILABILITY NOTICE

Availability of Reference Materials Cited in NRC Publications

Most documents cited in NRC publications will be available from one of the following sources:

1. The NRC Public Document Room, 2120 L Street, NW., Lower Level, Washington, DC 20555

2. The Superintendent of Documents, U.S. Government Printing Office, P.O. Box 37082, Washington, DC 20013-7082

3. The National Technical Information Service, Springfield, VA 22161

Although the listing that follows represents the majority of documents cited in NRC publications, it is not intended to be exhaustive.

Referenced documents available for inspection and copying for a fee from the NRC Public Document Room include NRC correspondence and internal NRC memoranda; NRC bulletins, circulars, information notices, inspection and investigation notices; licensee event reports; vendor reports and correspondence; Commission papers; and applicant and licensee documents and correspondence.

The following documents in the NUREG series are available for purchase from the GPO Sales Program: formal NRC staff and contractor reports, NRC-sponsored conference proceedings, international agreement reports, grant publications, and NRC booklets and brochures. Also available are regulatory guides, NRC regulations in the *Code of Federal Regulations*, and *Nuclear Regulatory Commission Issuances*.

Documents available from the National Technical Information Service include NUREG-series reports and technical reports prepared by other Federal agencies and reports prepared by the Atomic Energy Commission, forerunner agency to the Nuclear Regulatory Commission.

Documents available from public and special technical libraries include all open literature items, such as books, journal articles, and transactions. *Federal Register* notices, Federal and State legislation, and congressional reports can usually be obtained from these libraries.

Documents such as theses, dissertations, foreign reports and translations, and non-NRC conference proceedings are available for purchase from the organization sponsoring the publication cited.

Single copies of NRC draft reports are available free, to the extent of supply, upon written request to the Office of Administration, Distribution and Mail Services Section, U.S. Nuclear Regulatory Commission, Washington, DC 20555.

Copies of industry codes and standards used in a substantive manner in the NRC regulatory process are maintained at the NRC Library, 7920 Norfolk Avenue, Bethesda, Maryland, for use by the public. Codes and standards are usually copyrighted and may be purchased from the originating organization or, if they are American National Standards, from the American National Standards Institute, 1430 Broadway, New York, NY 10018.

DISCLAIMER NOTICE

This report was prepared as an account of work sponsored by an agency of the United States Government. Neither the United States Government nor any agency thereof, or any of their employees, makes any warranty, expressed or implied, or assumes any legal liability of responsibility for any third party's use, or the results of such use, of any information, apparatus, product or process disclosed in this report, or represents that its use by such third party would not infringe privately owned rights.

NUREG/CR-4667, Vol. 14
ANL-92/30
R5

Environmentally Assisted Cracking in Light Water Reactors

Semiannual Report
October 1991–March 1992

Manuscript Completed: July 1992
Date Published: August 1992

Prepared by
H. M. Chung, T. F. Kassner, S. Majumdar, J. Y. Park,
A. Purohit, W. J. Ruther, J. E. Sanecki, W. J. Shack

Argonne National Laboratory
9700 South Cass Avenue
Argonne, IL 60439

Prepared for
Division of Engineering
Office of Nuclear Regulatory Research
U.S. Nuclear Regulatory Commission
Washington, DC 20555
NRC FINs A2212, A2256

Previous Documents in Series

Light-Water-Reactor Safety Materials Engineering Research Programs: Quarterly Progress Report October--December 1984, NUREG/CR-3998 Vol. III, ANL-84-60 Vol. III (October 1985).

Light-Water-Reactor Safety Materials Engineering Research Programs: Quarterly Progress Report January--March 1985, NUREG/CR-4490 Vol. I, ANL-85-75 Vol. I (March 1986).

Environmentally Assisted Cracking in Light Water Reactors Semiannual Report April--September 1985, NUREG/CR-4667 Vol. I, ANL-86-31 (June 1986).

Environmentally Assisted Cracking in Light Water Reactors Semiannual Report October 1985--March 1986, NUREG/CR-4667 Vol. II, ANL-86-37 (September 1987).

Environmentally Assisted Cracking in Light Water Reactors Semiannual Report April--September 1986, NUREG/CR-4667 Vol. III, ANL-87-37 (September 1987).

Environmentally Assisted Cracking in Light Water Reactors Semiannual Report October 1986--March 1987, NUREG/CR-4667 Vol. IV, ANL-87-41 (December 1987).

Environmentally Assisted Cracking in Light Water Reactors Semiannual Report April--September 1987, NUREG/CR-4667 Vol. V, ANL-88-32 (June 1988).

Environmentally Assisted Cracking in Light Water Reactors Semiannual Report October 1987--March 1988, NUREG/CR-4667 Vol. 6, ANL-89/10 (August 1989).

Environmentally Assisted Cracking in Light Water Reactors Semiannual Report April--September 1988, NUREG/CR-4667 Vol. 7, ANL-89/40 (March 1990).

Environmentally Assisted Cracking in Light Water Reactors Semiannual Report October 1988--March 1989, NUREG/CR-4667 Vol. 8, ANL-90/4 (June 1990).

Environmentally Assisted Cracking in Light Water Reactors Semiannual Report April--September 1989, NUREG/CR-4667 Vol. 9, ANL-90/48 (March 1991).

Environmentally Assisted Cracking in Light Water Reactors Semiannual Report October 1989--March 1990, NUREG/CR-4667 Vol. 10, ANL-91/5 (March 1991).

Environmentally Assisted Cracking in Light Water Reactors Semiannual Report April--September 1990, NUREG/CR-4667 Vol. 11, ANL-91/9 (May 1991).

Environmentally Assisted Cracking in Light Water Reactors Semiannual Report October 1990--March 1991, NUREG/CR-4667 Vol. 12, ANL-91/24 (August 1991).

Environmentally Assisted Cracking in Light Water Reactors Semiannual Report April--September 1991, NUREG/CR-4667 Vol. 13, ANL-92/6 (March 1992).

Environmentally Assisted Cracking in Light Water Reactors

by

H. M. Chung, T. F. Kassner, S. Majumdar, J. Y. Park,
A. Purohit, W. E. Ruther, J. E. Sanecki, and W. J. Shack

Abstract

This report summarizes work performed by Argonne National Laboratory on fatigue and environmentally assisted cracking in light water reactors during the six months from October 1991 to March 1992. Fatigue and environmentally assisted cracking of piping, pressure vessels, and core components in light water reactors are important concerns as extended reactor lifetimes are envisaged. Topics that have been investigated during this year include (1) fatigue and stress corrosion cracking (SCC) of low-alloy steel used in piping and in steam generator and reactor pressure vessels, (2) radiation-induced segregation (RIS) and irradiation-assisted SCC of Type 304 SS after accumulation of relatively high fluence, and (3) update of a crack growth data base for austenitic and ferritic steels in high-temperature water. Existing data on fatigue of low-alloy steel in LWR environments have been reviewed. Based on fracture-mechanics models and engineering judgement, interim fatigue design curves are being developed that are consistent with available fatigue-life data. Microchemical and microstructural changes in high- and commercial-purity Type 304 SS specimens from control-blade absorber tubes and a control-blade sheath from operating BWRs were studied by Auger electron spectroscopy and scanning electron microscopy. Slow-strain-rate-tensile tests were conducted on irradiated specimens in air and in simulated BWR water at 289°C. Crack growth data on fracture-mechanics specimens of austenitic and ferritic steels in simulated BWR water, developed in this program over the past eight years, were compiled into a data base along with references that contain details of test methods, material compositions, metallographic information, and comparisons of data with predictions based on the new crack growth curves proposed for inclusion in Section XI of the ASME Code.

Contents

Figures

Tables

Executive Summary

Fatigue of Ferritic Piping and Pressure Vessel Steels

Plain carbon steels are used extensively in PWR and BWR nuclear steam supply systems as piping and pressure vessel materials. The steels of interest for these applications include A106-Gr B and A333-Gr 6 for seamless pipe and A302 Gr B, A508-2, and A533-Gr B plate for pressure vessels. Existing data in the literature on fatigue of low-alloy steels in LWR environments have been reviewed. Both temperature and dissolved-oxygen concentration in water have a significant effect on fatigue life. In oxygenated water, fatigue life depends strongly on strain rate; alternatively, the dependence on loading history can be characterized in terms of frequency or rise time. For the same environment and strain range, lives can vary by a factor of 100, depending on strain rate. When data are extrapolated to strain rates characteristic of realistic reactor transients (often $<10^{-6}$ s^{-1}), predicted reductions in fatigue life are by factors of ~1000 or more. However, the relatively good service experience of carbon steel piping in BWRs indicates that extrapolation to such low strain rates is unrealistic and that the effect of strain rate on fatigue life must saturate at some level, although no such saturation has been observed in laboratory tests conducted to date. Ongoing tests at ANL should resolve this issue. Based on fracture-mechanics models and engineering judgment, interim fatigue design curves are being developed and are consistent with available data.

Stress Corrosion Cracking of Ferritic Steels

Additional fracture-mechanics CGR tests have been performed on nonplated specimens of A106-Gr B and A533-Gr B steel and on specimens of A533-Gr B plated with nickel-chromium. The effect of frequency on CGRs was determined at a load ratio of 0.2 in high-purity oxygenated (~200 ppb) water at 289°C. The CGRs for the nickel-chromium-plated A533-Gr B specimen were compared with predicted values from the new correlations proposed for inclusion in Section XI of the ASME Boiler and Pressure Vessel Code. The proposed Section XI correlations were nonconservative for data obtained at long rise times.

Irradiation-Assisted Stress Corrosion Cracking of Type 304 SS

Failures of austenitic stainless steel (SS) after accumulation of high fluence have been attributed to radiation-induced segregation (RIS) or depletion of elements such as Si, P, S, Ni, and Cr. However, the exact identity of the elements that segregate and the degree to which RIS produces susceptibility of the core internal components of LWRs to irradiation-assisted SCC are unclear. High- and commercial-purity (HP and CP, respectively) Type 304 SS specimens were obtained from neutron-absorber tubes and a control-blade sheath irradiated in commercial BWRs. SSRT tests were conducted on irradiated specimens in air and in simulated BWR water at 289°C. SCC susceptibility of the sheath was significantly lower than those of neutron-absorber tubes fabricated from another CP grade and from that exhibited by two HP-grade heats of Type 304 SS examined in previous investigations. Grain-boundary segregation of impurities in the CP sheath and CP neutron-absorber tube was comparable, except for an indication of C segregation and a higher level of grain-boundary Cr in the sheath material. SCC susceptibility of BWR components fabricated from

CP and HP heats of Type 304 SS could not be correlated with grain-boundary segregation of Si, P, or S. The relative SCC susceptibility of the HP and CP absorber tubes and the CP sheath could be correlated with minimum grain-boundary Cr contents that were determined by an Auger electron spectroscopy depth-profiling technique.

Crack Growth Data Base for Austenitic and Ferritic Steels

Crack growth tests have been conducted on fracture-mechanics specimens of Types 304, 316NG, and 347 SS and A106-Gr B and A533-Gr B ferritic steel to characterize environmental, loading, and material conditions that can produce SCC susceptibility in these steels. Data that have been obtained over the past eight years (October 1983 to September 1991) are summarized along with references that contain details of the test methods, composition of the materials, metallographic and fractographic information, and comparisons of the data with predictions of Section XI of the ASME Code. CGR tests are in progress on specimens of CF-3, CF-3M, CF-8, and CF-8M grades of cast SS in the as-received and thermally aged conditions. Tests on specimens of A106-Gr B and A533-Gr B steel are being continued to quantify the effects of material chemistry, load history, and dissolved-oxygen content of simulated BWR and PWR secondary-system water on SCC.

1 Introduction

Fatigue and environmentally assisted cracking of piping, pressure vessels, and core components in light water reactors (LWRs) are important concerns as extended reactor lifetimes are envisaged. The degradation processes include intergranular stress corrosion cracking (IGSCC) of austenitic stainless steel (SS) piping in boiling water reactors (BWRs), and propagation of fatigue or SCC cracks (which initiate in sensitized SS cladding) into low-alloy ferritic steels in BWR pressure vessels.* Similar cracking has also occurred in upper-shell-to-transition-cone girth welds in pressurized water reactor (PWR) steam generator vessels,** and cracks have been found in steam generator feedwater distribution piping.*** Another concern is failure of reactor-core internal components after accumulation of relatively high fluence, which has occurred in both BWRs and PWRs. The general pattern of the observed failures indicates that, as nuclear plants age and the neutron fluence increases, a wide variety of apparently nonsensitized austenitic materials become susceptible to intergranular failure by a degradation process commonly known as irradiation-assisted stress-corrosion cracking (IASCC). Some of the failures have been reported for components that are subjected to relatively low or negligible stress levels, e.g., control-blade sheaths and handles and instrument dry tubes of BWRs. Although most failed components can be replaced, some safety-significant structural components, such as the BWR top guide, shroud, and core plate, would be very difficult or impractical to replace. Research during the past six months has focused on (1) fatigue and SCC of ferritic steels used in piping and in steam generator and reactor pressure vessels and (2) IASCC in high- and commercial-purity Type 304 SS specimens from control-blade absorber tubes and a control-blade sheath used in operating BWRs. Crack growth data on austenitic and ferritic steels in simulated BWR water developed in this program over the past eight years has been compiled into a data base.

2 Fatigue of Ferritic Steels

2.1 Technical Progress (S. Majumdar and W. J. Shack)

The existing data in the literature on the fatigue of carbon steel in LWR environments have been reviewed. The primary published sources of this data are the work by Higuchi and Iida,[1] the data obtained in a test loop at the Dresden 1 reactor by GE,[2,3] and tests performed by GE/EPRI,[4] and the work by Terrell.[5] In addition, tests have been conducted in water chemistries characteristic of fossil-fired power generation systems by B&W.[6] Although these water chemistries are much different than LWR coolant chemistries, the temperature and oxygen levels, which appear to be the critical environmental variables, are in the ranges of interest.

*USNRC Information Notice No. 90-29, "Cracking of Cladding in Its Heat Affected Zone in the Base Metal of a Reactor Vessel Head," April 30, 1990.

**USNRC Information Notice No. 90-04, "Cracking of the Upper Shell-to-Transition Cone Girth Welds in Steam Generators," January 26, 1990.

***USNRC Information Notice No. 91-19, "Steam Generator Feedwater Distribution Piping Damage," March 12, 1991.

Several trends are clear from the available data. Both temperature and dissolved-oxygen concentration in water have a significant effect on fatigue life. At the very low dissolved-oxygen levels characteristic of PWRs and BWRs with hydrogen-water chemistry, environmental effects on fatigue life are modest. At dissolved-oxygen levels ≥100 ppb, significant reductions in fatigue life can occur. The effect of dissolved-oxygen level saturates at ≈200 ppb and fatigue life does not decrease significantly with oxygen concentration over the range ≈0.2–8 ppm. In oxygenated water, fatigue life depends strongly on strain rate; alternatively, the dependence on loading history can also be characterized in terms of frequency or rise time. For the same environment and strain range, lives can vary by a factor of 100, depending on strain rate.

2.1.1 Empirical Correlations for Effect of Environment on Fatigue Life

Higuchi & Iida[1] correlate their data by assuming that life in the environment is related to life in air through a power-law dependence on strain rate:

$$N_{water} = N_{air}\,(\dot{\varepsilon})^{p} \tag{1}$$

The strain-rate exponent p is a function of temperature (T) and dissolved-oxygen level (O). The best fit to the data is obtained in terms of a piecewise linear relationship of the form:

$$p = p_0 + M(O)\cdot N(T) \tag{2}$$

where

$$M(O) = \begin{cases} m_l & O \le O_l \\ m_l + (m_h - m_l)\cdot\dfrac{(O - O_l)}{(O_h - O_l)} & O_l < O \le O_h \\ m_h + k_O\cdot(O - O_h) & O_h < O \end{cases} \tag{3}$$

and

$$N(T) = \begin{cases} k_{100}\cdot\dfrac{T}{100} & T \le 100 \\ k_{100} + (k_{200} - k_{100})\cdot\dfrac{(T - 100)}{100} & 100 < T \le 200 \\ k_{200} + (k_{300} - k_{200})\cdot\dfrac{(T - 200)}{100} & 200 < T \end{cases} \tag{4}$$

Specific values for the constants, p_0, m_l, O_l, etc., for strain rates expressed in %/s, chosen by Higuchi & Iida,[1] are given in Table 1.

Table 1. Coefficients in Piecewise Linear Correlation for Strain-Rate Exponent p

	p_0	m_l	O_l	m_h	O_h	k_0	k_{100}	k_{200}	k_{300}
Higuchi & Iida	0.1	0	0.1	1	0.2	0	0.2	0.2	0.6
Optimized Fit	0.1	0.00	0.09	0.99	0.23	0.02	0.14	0.14	0.63
Modified	0.1	0	0.1	1	0.2	0.02	0.15	0.15	0.6

No details on the choice of the coefficients are given in Ref. 1. However, if all coefficients in the piecewise-linear correlations are determined by minimizing differences between predicted and observed lives in the tests in Ref. 1, the results are very close to those given in Ref. 1, as shown in Table 1. A simplified and slightly more conservative choice of coefficients is shown in row 3 of Table 1. A comparison between predicted and observed lives for the three correlations is shown in Fig. 1. Only low-strain-rate data are shown in the figure. The scatter increases slightly when all data in Ref. 1 are included. Several other analytical forms for fitting the data were examined, but the piecewise-linear form (Eq. 1) was the most successful.

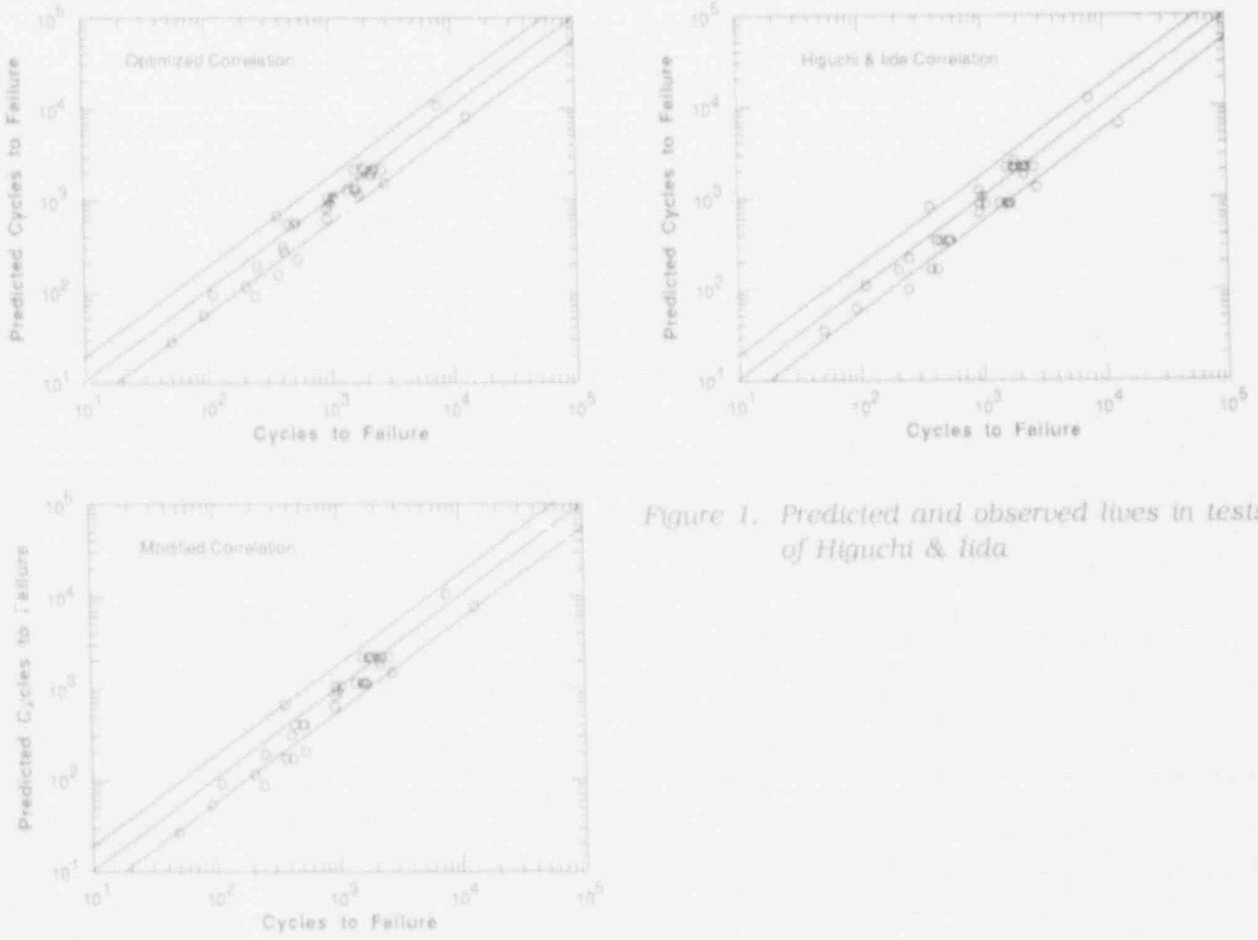

Figure 1. Predicted and observed lives in tests of Higuchi & Iida

The variation of the strain-rate exponent with temperature and dissolved-oxygen level is shown in Fig. 2 for the correlation of Higuchi & Iida[1] and the modified version given in

Table 1. Differences between the two correlations are slight. The strong dependence on oxygen level below 200 ppb and the relatively weak dependence at higher levels are consistent with the results of Nagata et al.[7] (on low-alloy steels) and B&W.[6] At 200 ppb dissolved oxygen and 288°C, both correlations give virtually identical values. Lives predicted by these correlations and data obtained at Dresden[2] are shown in Fig. 3. The predicted and observed lives are in good agreement.

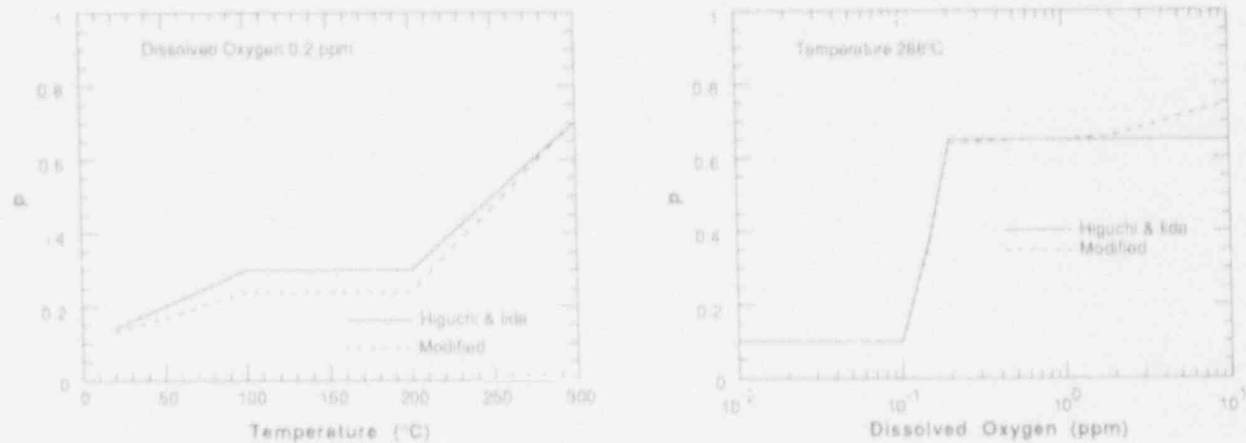

Figure 2. Variation of strain rate exponent p with temperature at a dissolved-oxygen level of 200 ppb and variation of p with dissolved-oxygen level at 288°C

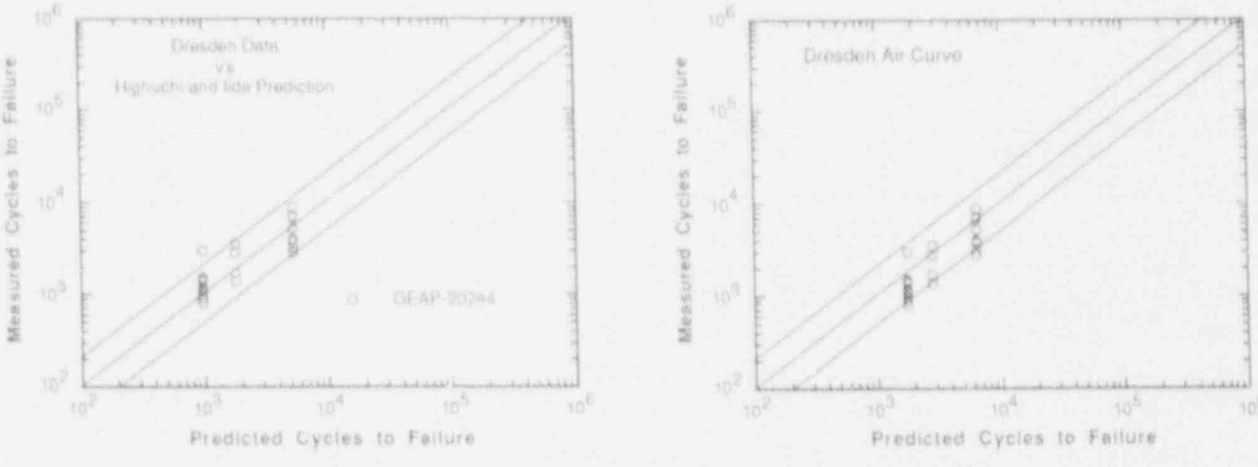

Figure 3. Comparison of predicted lives with those in GE tests at Dresden and laboratory tests under load control. In (a), predictions are based on air data of Higuchi & Iida; in (b) the reference curve is 288°C air data for material in Dresden tests.

Applied strain rate in Eq. 1 has a critical effect on fatigue life. In water containing 200 ppb dissolved oxygen at 288°C, the strain rate exponent p is ≈0.6. Strain rates for laboratory and in-reactor tests at Dresden are higher than those of typical reactor transients. By using Eq. 1 to extrapolate to strain rates characteristic of realistic transients (often 10^{-6} s^{-1} or less), predicted reductions in fatigue life are by factors of ≈1000 or more.

The relatively good service experience of carbon steel piping in BWRs indicates that extrapolation of the power-law relation (Eq. 1) to such low strain rates is unrealistic and that the effect of strain rate on fatigue life must saturate at some level, although no such saturation has been observed in laboratory tests conducted to date. Equation 1 also appears to be physically unsatisfactory in another respect. It suggests that the relative shift in fatigue life is independent of strain range and depends only on strain rate. Indeed for a fixed rise time or frequency, it suggests that the relative effect would be larger at lower strain ranges because the strain rate would be lower. This seems contrary to an intuitive expectation that the effect of environment should be a function of plastic strain in the material, i.e., environmental effects should diminish as plastic deformation decreases.

The data currently available at very low strain rates and/or low strain ranges are insufficient for empirical demonstration of saturation at low strain rates and the diminished effect of the environment at low strain ranges. We are developing interim fatigue design curves that are consistent with available data based on fracture-mechanics models and engineering judgment rather than rely on a purely empirical relation such as Eq. 1.

2.1.2 Development of Model for Prediction of Fatigue Lives

Life of a "smooth" fatigue specimen has long been recognized to consist of a crack nucleation phase and a crack growth phase. At low strain ranges, life is dominated by crack nucleation, whereas crack growth dominates life at high strain ranges. Crack nucleation is controlled by the strength of the material and is assumed to depend primarily on applied stress range (or elastic strain range). On the other hand, low-cycle (crack growth) fatigue life is controlled by ductility of the material and depends primarily on applied plastic strain range. The data of Terrell[5] have been used to estimate the mean fatigue life of a carbon steel (A106-Gr B) at 288°C in air. This mean-data curve is shown in Fig. 4a, which also includes estimated crack nucleation and crack propagation life curves based on the assumptions that nucleation life depends on applied elastic strain range and that propagation life depends on applied plastic strain range. Although the fatigue curves in Fig. 4a were obtained from fatigue and cyclic stress-strain data of Terrell,[5] the fatigue curve is not significantly different from the mean-data curve used to generate the design fatigue curve in Section III of the ASME Code.[8] Hence, the nucleation and propagation life curves are assumed to be reasonable estimates of the mean-data curves for carbon steels.

Dowling[9] has demonstrated that by characterizing the fracture-mechanics crack-growth rate in terms of ΔJ, fracture-mechanics analyses can be used to develop estimates of fatigue life at high strain ranges by computing the number of cycles required to grow from an initial flaw size a_o to failure. Using the in-air crack-growth-rate curve given in the current proposed revision to Section XI of the ASME Code,[10] we obtained good agreement between the model lives predicted by Dowling's model[9] and actual fatigue lives for an initial flaw a_o of 0.18 mm. The propagation life at any strain range can be calculated by computing the number of cycles required to grow from this initial flaw to a final crack size of 2.54 mm. The crack nucleation life N_i can then be interpreted as the number of cycles needed to nucleate a crack of size ≈0.18 mm and corresponds to the difference between the actual life and the propagation life computed from the crack propagation model. N_i is a function of

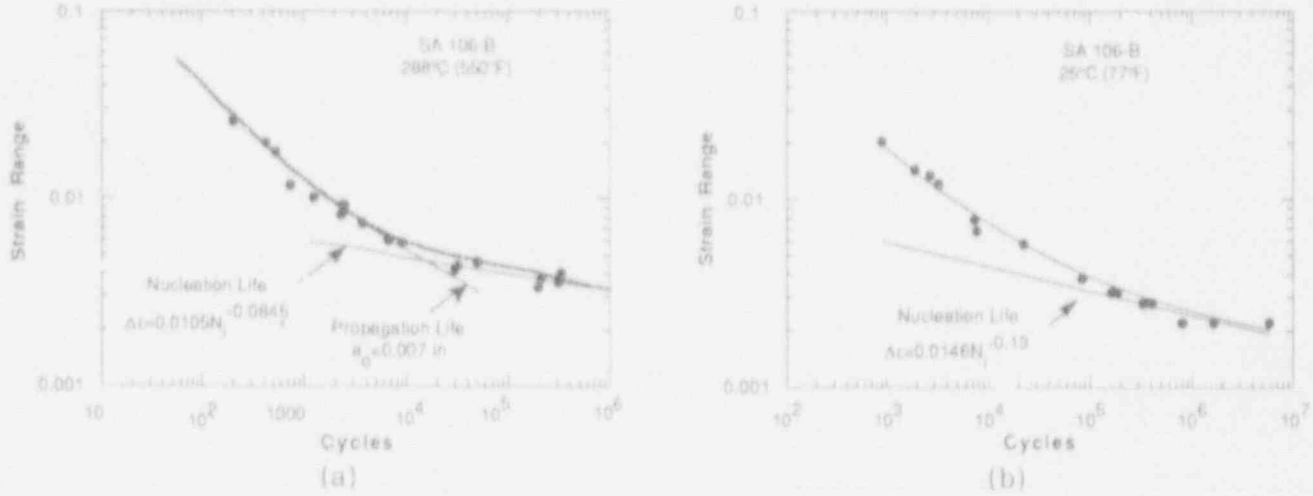

Figure 4. Fatigue curves for a carbon steel tested in air at 288°C and room temperature

applied stress range $\Delta\sigma$, although it can also be expressed in terms of applied strain range through the cyclic stress–strain curve; for A106–Gr B steel at 288°C in air, a power-law best fit gives

$$\Delta\sigma = 2{,}000N_i^{-0.0845} \tag{5a}$$

or

$$\Delta\varepsilon = 0.0105N_i^{-0.0845} \tag{5b}$$

At room temperature, the crack nucleation life is given by (Fig. 4b):

$$\Delta\sigma = 3020N_i^{-0.13} \tag{6a}$$

or

$$\Delta\varepsilon = 0.0146N_i^{-0.13} \tag{6b}$$

The crack propagation life N_p in air at 288°C and at room temperature can be expressed in terms of strain range

$$\Delta\varepsilon = 0.210N_p^{-0.4055} \tag{7}$$

and

$$\Delta\varepsilon = 0.244N_p^{-0.3758}. \tag{8}$$

Crack propagation life in water is obtained by calculating the number of cycles required to grow from a_o to failure with the crack-growth-rate curve for carbon steels in LWR water currently being proposed for inclusion in Section XI of the Code.[10] The total life N_f can then be expressed as the sum of the crack nucleation and crack propagation (N_p) lives

$$N_f = N_i + N_p \tag{9}$$

Terrell[5] has noted that carbon steels, e.g., A106–Gr B, exhibit strain aging at reactor operating temperatures. Tensile tests on A333–Gr 6 and A106–Gr B specimens obtained from pipes of various diameters have shown that the magnitude of the strain aging peak of the ultimate tensile strength (UTS) can vary significantly (by factors of ≈1.09–1.30 relative to the UTS at room temperature) for the same grade of material.[11] Examination of the data of Higuchi on A333–Gr 6 steel contained in the FADAL data base also clearly demonstrates an increase in stress range with decreasing strain rate (Fig. 5), which may be caused by a strain aging effect. The increase in UTS caused by strain aging is accompanied by a decrease in ductility, as measured by reduction in area or elongation. Consequently, low–cycle fatigue life can decrease as strain rate decreases in the temperature range where dynamic strain aging occurs.[12] Conversely, because high–cycle fatigue life depends on the strength of the material, life is expected to increase as the strain rate decreases. Terrell's[5] data do show that stress versus fatigue–life curves (at 4×10^{-3} s^{-1}) at room temperature and at 288°C cross over in the high–cycle fatigue regime.

In addition to dynamic strain aging, environmental degradation of high–cycle fatigue life can also occur from surface pitting. Even in the absence of macroscopic pitting, such pits, which appear to occur at the sites of MnS particles in carbon and low–sulfur low–alloy steels in oxygenated water, will cause stress concentrations and consequently reduce the high–cycle fatigue life. An examination of a A106–Gr B specimen tested to failure at a strain range of 0.75% in 288°C water containing 300 ppb dissolved oxygen revealed several cracks that initiated at pits, including the one that led to fracture. The data of Higuchi and Iida[1] include tests at strain ranges as low as 0.4% which show a significant degradation in fatigue life. The tests by E&W[6] in oxygenated secondary–side water chemistries at a strain range of 0.5% also show a more significant effect of environment than would be expected on the basis of a decrease in crack propagation life alone.

To summarize, crack nucleation life (high–cycle fatigue) is expected to increase and crack propagation life (low–cycle fatigue) is expected to decrease as strain rate decreases because of strain aging effects at 100–288°C. Because crack nucleation life constitutes a small fraction of total life at high strain ranges, the net effect of strain aging on low–cycle fatigue life is detrimental. Although strain aging may tend to increase high–cycle fatigue life at 100–288°C, stress concentration effects from surface pits that form on the steel in oxygenated water will reduce high–cycle fatigue life. The net effect of these two competing processes may vary from heat to heat and will depend on material composition, dissolved–oxygen level, temperature, and exposure history. Available data are not adequate to accurately characterize crack nucleation life in terms of all relevant variables. At present, pitting is assumed to occur in oxygenated water and produce a net effective stress concentration factor (k_f) of 1.2. No benefit is assumed for the improvement in high–cycle fatigue life due to strain aging. These assumptions are consistent with limited data at relatively low strain ranges.[1,5]

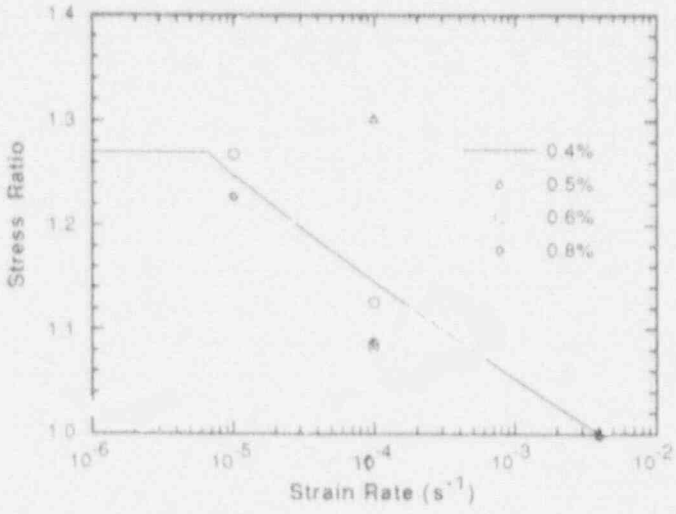

Figure 5. Dependence of cyclic stress ratio at several strain amplitudes on strain rate for a carbon steel at 250°C

2.1.3 Model Predictions and Comparison with Experimental Results

Figure 6 shows predicted lives at a strain range of 1.2% as a function of strain rate, along with data of Higuchi and Iida[1] at this strain range in water containing 8 ppm dissolved oxygen at 290°C. Predicted lives are computed with the proposed Section XI crack-growth curves at 288°C where a threshold effect on environmentally assisted cracking (EAC) is observed, and at ≤277°C where the threshold may be absent.* Because of the high strain range, inclusion or neglect of a crack nucleation life makes no difference in predicted total life. Predicted and observed lives agree fairly well when no EAC threshold is assumed. For strain rates $>10^{-5}$ s^{-1}, the dependence is similar to the power-law dependence obtained from the empirical relation Eq. 1. Below 10^{-5} s^{-1}, the decrease in life with decreasing strain rate is predicted to saturate or even increase for the case where crack growth exhibits an EAC threshold. Such behavior has been reported in some Russian tests.[13]

At a strain range of 0.6%, inclusion or neglect of crack nucleation life has a large influence on predicted total life, as shown in Fig. 7. If no loss in crack nucleation life in water is assumed, predicted lives become increasingly nonconservative as strain rate decreases. An analysis that assumes zero crack nucleation life and no threshold in EAC predicts lives that are in good agreement with available experimental data. Saturation is again predicted at strain rates $<10^{-5}$ s^{-1}. Also, as before, predictions of a crack growth

* E. D. Eason, da/dN Data Analysis Update and Implications for S-N Data Analysis, Presentation at PVRC Workshop Cyclic Life and Environmental Effects in Nuclear Applications, Clearwater Beach, FL (January 20–21, 1992).

model without an EAC threshold appear to be more consistent with experimental data than a crack growth model with an EAC threshold. Consequently, we have used the crack growth model without an EAC threshold for the prediction of crack propagation lives.

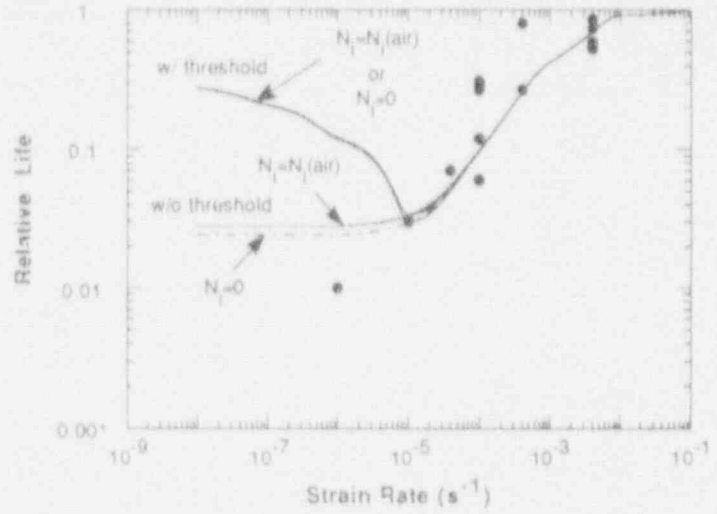

Figure 6. Predicted and observed fatigue lives of carbon steel as a function of strain rate for tests at a strain range of 1.2% in 288°C water containing 8 ppm dissolved oxygen

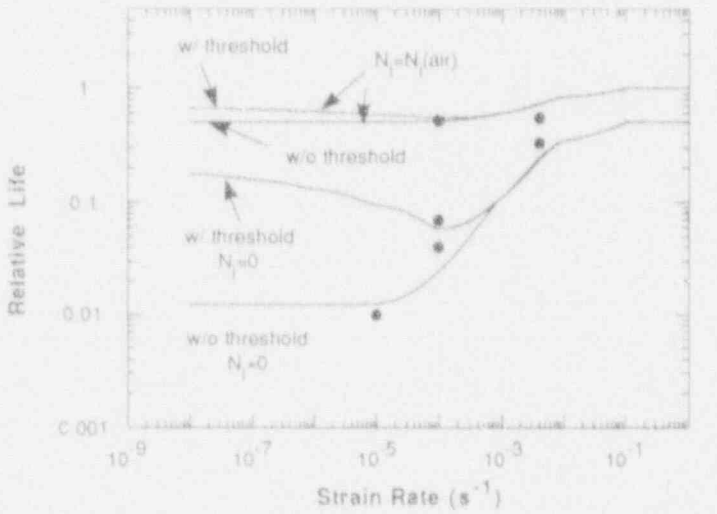

Figure 7. Predicted and observed fatigue lives of a carbon steel as function of strain rate for tests at a strain range of 0.6% in 288°C water containing 8 ppm dissolved oxygen

Predicted lives at a strain range of 0.5% are compared in Fig. 8 with fatigue data on carbon steels in water containing ≥0.3 ppm oxygen at 290°C.[6] Although the water chemistry for these tests is characteristic of fossil-fired secondary systems, the dissolved oxygen and temperature appear to be the most critical environmental variables. The assumption of no loss of crack nucleation life in water leads to increasingly non-conservative predicted lives as strain rate decreases. An analysis that assumes zero crack nucleation life underestimates the experimental lives. Better agreement between predicted and experimental lives can be obtained if the crack nucleation life is decreased by a factor of ≈100, which suggests that a recovery of the crack nucleation life may occur at a lower strain range.

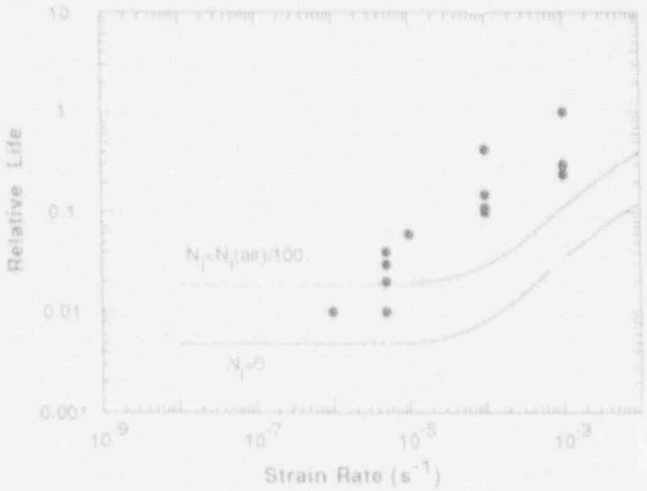

Figure 8. Predicted and observed fatigue lives of a carbon steel as a function of strain rate for tests at a strain range of 0.5% in 288°C water containing ≥300 ppb oxygen

The few data available at a strain range of 0.4%[1] are compared with predicted lives in Fig. 9. If crack nucleation life is assumed to be zero, as appears to be the case at higher strain ranges, predicted lives are much lower than experimental values. Figure 9 also shows that predicted lives based on a reduction in crack nucleation life by a factor of 10 are in better agreement with experimental results than lives based on a reduction factor of 100. Comparison of Figs. 8 and 9 tends to reinforce the notion that a recovery of crack nucleation life occurs with decreasing strain range, although more data are needed to better determine N_i at low strain ranges.

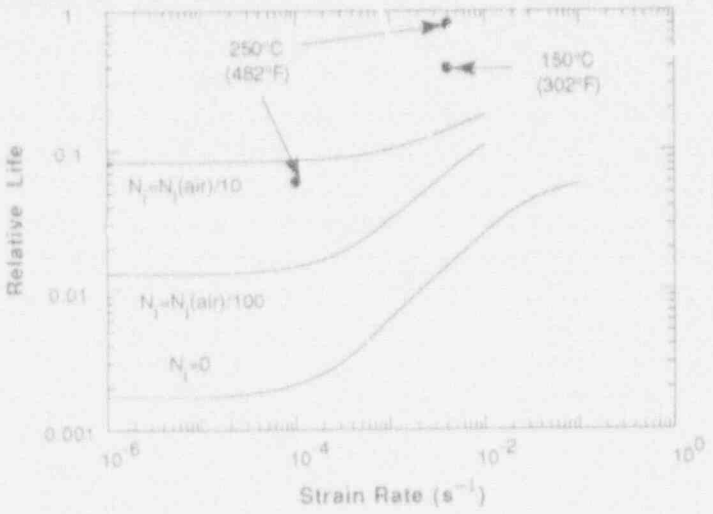

Figure 9. Predicted and observed fatigue lives of a carbon steel as function of strain rate for tests at a strain range of 0.4% in water containing 8 ppm oxygen.

3 Environmentally Assisted Cracking of Ferritic Steels

Over the past 15 years, the corrosion fatigue properties of low-alloy steels in LWR primary-system water chemistries have been studied extensively.[14-17] Much less information is available on SCC of these materials.[18-22] Because it is clear that very high crack-growth rates (CGRs) can occur in some materials under some combinations of loading and environment, the objective of the current work is to better define the circumstances that can produce SCC in these steels.

3.1 Technical Progress

Fracture-mechanics CGR tests have continued on compact-tension specimens from low- and medium-sulfur-content heats (0.004 and 0.018 wt.%) of A533-Gr B pressure vessel steel and a medium-sulfur-content (0.014%) A106-Gr B piping steel. One of the A533-Gr B specimens was nickel-chromium plated to better simulate a clad ferritic steel vessel, where only the low-alloy steel at the crack surface is exposed to the environment. Surface films on the nickel-chromium and on nickel- and gold-plated specimens tested previously[23,24] are different from those on the nonplated ferritic specimens. Because virtually all of the existing data have been obtained on specimens without cladding, it is important to verify that those results were not unduly affected by the character of the surface film.

3.1.1 Crack-Growth-Rate Tests on Ferritic Steel Specimens (J. Y. Park)

CGR tests were conducted on a set of three 1TCT carbon steel specimens (Nos. CTW7-03, 02C-07, and CTJ7-01). Specimens CTW7-03 and 02C-07 were prepared from a plates of a low- and high-sulfur A533-Gr B pressure vessel steels (Heat Nos. A5401, [0.004% S and 0.005% P] and A-1195-1 [0.018% S and 0.012% P]), respectively, and specimen CTJ7-01 was from a A106-Gr B piping steel (Heat No. J72X, [0.014% S and 0.014% P]). Specimen 02C-07 was plated with nickel-chromium to simulate austenitic SS cladding on a reactor pressure vessel, and hence, to determine the validity of using data obtained from specimens without cladding to analyze the behavior of a clad ferritic vessel where only the crack surface is exposed to the environment. In previous CGR tests, plated specimens showed greater susceptibility to SCC than did a conventional specimen.

The tests were performed in deionized water at 289°C under a cyclic load (sawtooth wave shape with 12- and 60-s loading and 1-s unloading time) at R values of 0.2-0.7 and frequencies of 1.6×10^{-2} and 7.7×10^{-2} Hz. Initial K_{max} values were 20, 23, and 20 MPa·m$^{1/2}$ for specimens CTJ7-01, 02C-07, and CTW7-03, respectively. A dissolved-oxygen concentration of 200-300 ppb in the effluent water from the autoclave was maintained by feedwater with 2-3 ppm oxygen. Crack length measurements were made by the DC potential-drop method. The results in Table 2 show that crack growth occurred at rates of 1.1×10^{-10} to 2.3×10^{-7} m·s^{-1} for the Ni-Cr plated specimen 02C-07, while nonplated specimens CTW7-03 and CTJ7-01 exhibited cracking during three or four of the test conditions. The maximum load was decreased at the end of Test 7 because the K_{max} value for the Ni-Cr plated specimen (02C-07) was quite high (91 MPa·m$^{1/2}$) due to the relatively long crack in this specimen. Crack growth resumed in the Ni-Cr plated specimen at K_{max} values between ~44 and 80 MPa·m$^{1/2}$; however, no cracking occurred in the two nonplated specimens at a K_{max} of <20 MPa·m$^{1/2}$. Because the crack length in the Ni-Cr plated specimen (02C-07) attained the maximum allowable length, the experiment was terminated and specimen 02C-07 was replaced with an identical Ni-Cr plated specimen (02C-14).

Tests on the three specimens were continued in deionized water at 289°C under cyclic loading (sawtooth wave shape with 12- to 3000-s loading and 1-s unloading time) at R = 0.2 and frequencies in a range 3.33×10^{-4} to 7.69×10^{-2} Hz. Initial K_{max} values were 26, 21, and 23 MPa·m$^{1/2}$ for specimens CTJ7-01, 02C-14, and CTW7-03, respectively. The results in Table 3 show that crack growth occurred at rates of 1.3×10^{-10} to 5.9×10^{-9} m·s^{-1} for the Ni-Cr plated specimen 02C-14, while no significant crack growth occurred for nonplated specimens CTW7-03 and CTJ7-01, as in the previous experiment. The CGRs of the four specimens at an R-value of 0.2 and rise times of 12 and 60 s (Tables 2 and 3) are shown in Fig. 10. For comparison, rates predicted by the proposed ASME Code Section XI[10] correlation are also included in the figure. The predicted and measured rates are in reasonable agreement; the predicted values for threshold for the onset of cracking are lower (conservative) by ~5 MPa·m$^{1/2}$. The dependence of the CGRs of specimen 02C-14 on frequency at a R-value of 0.2 from the data in Table 3 is shown in Fig. 11. Rates predicted by the proposed ASME Code Section XI correlation[10] are also included in this figure. The observed CGRs are faster than the predicted values at rise times between 25 and 1500 s. The CGR at a rise time of 400 s is greater by an order of magnitude than the predicted value. At rise times outside of this range, the observed CGRs were bounded by

Table 2. Crack Growth of A533–Gr B Steel and A106–Gr B 1T–Compact Tension Specimens[a] under Cyclic Loading[b] in 289°C Water[c] Containing ≈200–300 ppb Dissolved Oxygen

Test No.	Time, h	Cond., μS·cm^{-1}	Potential Pt, mV(SHE)	Load Ratio	Freq., 10^{-2} Hz	Rise Time, s	A106–Gr B (No. CTJ7–01) Nonplated K_{max}[d], MPa·m$^{1/2}$	A106–Gr B (No. CTJ7–01) Nonplated Rate, 10^{-10} m·s^{-1}	A533–Gr B (No. 02C–07) Ni–Cr Plated K_{max}[d], MPa·m$^{1/2}$	A533–Gr B (No. 02C–07) Ni–Cr Plated Rate, 10^{-10} m·s^{-1}	A533–Gr B (No. CTW7–03) Nonplated K_{max}[d], MPa·m$^{1/2}$	A533–Gr B (No. CTW7–03) Nonplated Rate, 10^{-10} m·s^{-1}
1	1012	0.19	281	0.2	7.7	12	19.8	13	23.1	390	26.1	55.0
2	1031 1032	0.19	271	0.2	7.7	12	28.3	320	41.5	780	26.3	100.0
3	1049 1050	0.20	274	0.2	1.6	60	29.0	200	46.0	930	26.4	-
4	1052 1052	0.07	283	0.2	1.6	60	29.2	-	49.9	1300	-	-
5	1054 1054	0.07	278	0.2	1.6	60	29.5	-	55.3	1600	-	-
6	1056 1056	0.07	277	0.2	1.6	60	29.7	-	65.2	2300	26.5	20
7	1058 1062	0.07	268	0.7	1.6	60	30.1	2	91.0	120	26.6	-
8	1076 1078	0.22	279	0.7	7.7	12	14.9	-	43.9	-	13.2	-
9	1173 1174	0.21	256	0.7	7.7	12	19.7	-	60.5	-	17.6	-
10	1371 1371	0.11	286	0.6	7.7	12	-	-	-	-	17.5	-
11	1417 1418	0.14	296	0.5	7.7	12	-	-	60.0	1.1	17.5	-
12	1537 1556	0.22	294	0.4	7.7	12	19.6	-	61.5	36	17.5	-
13	1562 1562	0.22	294	0.4	7.7	12	19.7	-	62.2	110	17.5	-
14	1564 1564	0.22	292	0.4	7.7	12	19.6	-	63.1	160	17.5	-
15	1566 1566	0.22	289	0.4	7.7	12	19.6	-	64.5	230	17.5	-
16	1568 1568	0.22	292	0.4	7.7	12	19.6	-	68.3	590	17.5	-
17	1570 1570	0.18	292	0.4	7.7	12	19.6	-	79.9	1500	17.5	-

[a]Heats No. J7201 for A106 Gr–B (Specimen No. CTJ7–01), A–1195–1 for A533–Gr B (Specimen No. 02C–07) and A5401 for A533–Gr B (Specimen No. CTW7–03). Crack plane orientation was the L–T direction.

[b]Positive sawtooth wave form was used.

[c]Effluent dissolved-oxygen concentration was ≈200–300 ppb; feedwater oxygen concentration was approximately an order of magnitude higher to compensate for oxygen depletion by corrosion of the autoclave system.

[d]Stress intensity, K_{max}, values at the end of the time period.

Table 3. Effect of Frequency[a] on Crack Growth of A533-Gr B and A106-Gr B 1T-Compact Tension Specimens[b] in 289°C Water Containing ≈200-300 ppb Dissolved Oxygen[c]

Test No.	Time, h	Cond., μS cm^{-1}	Potentials A533-Gr B, Pt. mV(SHE)		Load Ratio	Rise Freq., 10^{-2} Hz	Rise Time, s	A106-Gr B [No. CTJ7-01] Nonplated K_{max}[d], MPa m$^{1/2}$	A106-Gr B [No. CTJ7-01] Nonplated Rate, 10^{-10} m s^{-1}	A533-Gr B [No. 02C-14] Ni-Cr Plated K_{max}[d], MPa m$^{1/2}$	A533-Gr B [No. 02C-14] Ni-Cr Plated Rate, 10^{-10} m s^{-1}	A533-Gr B [No. CTW7-03] Nonplated K_{max}[d], MPa m$^{1/2}$	A533-Gr B [No. CTW7-03] Nonplated Rate, 10^{-10} m s^{-1}
1	1205 1212	0.08	153	231	0.2	7.7	12	25.5	–	21.3	52	22.5	–
2	1214 1220	0.08	159	231	0.2	3.9	25	25.5	–	21.4	54	22.5	–
3	1222 1229	0.08	138	227	0.2	2.0	50	25.5	–	21.6	36	22.4	–
4	1230 1242	0.08	154	238	0.2	0.9	100	25.5	3	21.8	29	22.4	1.1
5	1244 1252	0.08	181	259	0.2	0.5	200	25.5	–	21.9	27	22.4	–
6	1254 1262	0.09	187	251	0.2	0.3	400	25.5	–	21.9	21	22.4	–
7	1263 1272	0.07	183	250	0.2	0.13	750	25.5	3	22.0	8	22.4	1.5
8	1273 1322	0.08	159	237	0.2	0.07	1500	25.5	–	22.0	1.3	22.4	–
9	1324 1459	0.09	148	224	0.2	0.03	3000	25.5	–	22.1	–	22.5	–
10	1461 1484	0.10	153	222	0.2	3.9	25	25.6	–	22.2	–	22.5	–
11	1485 1490	0.10	146	221	0.2	7.7	12	25.6	–	22.3	59	22.5	–

[a]Positive sawtooth wave form was used.

[b]Heats No. J7201 for A106 Gr-B [Specimen No. CTJ7-01], A-1195-1 for A533-Gr B [Specimen No. 02C-14] and A5401 for A533-Gr B [Specimen No. CTW7-03]. Crack plane orientation was the L-T direction.

[c]Effluent dissolved-oxygen concentration was ≈200-300 ppb; feedwater oxygen concentration was approximately an order of magnitude higher to compensate for oxygen depletion by corrosion of the autoclave system.

[d]Stress intensity, K_{max}, values at the end of the time period.

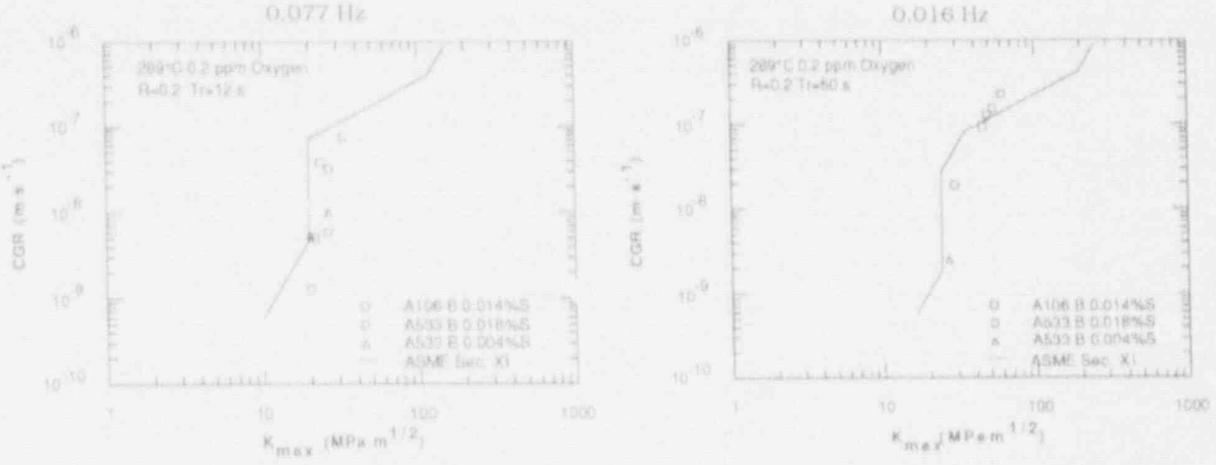

Figure 10. Crack growth rates vs. maximum stress intensity for A533-Gr B (0.004% S), Cr-Ni plated A533-Gr B (0.018% S), and A106-Gr B (0.014% S) specimens at R = 0.2 and 0.077 and 0.016 Hz in high-purity oxygenated water at 289°C

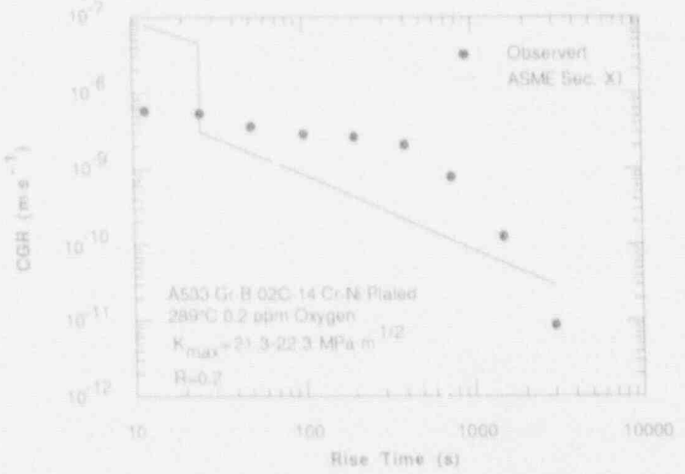

Figure 11. Crack growth rates vs. rise time for Cr-Ni plated A533-Gr B (0.018% S) steel at R = 0.2 in high-purity oxygenated water at 289°C

the ASME correlation. The magnitude of environmental enhancement predicted by the correlation is adequate to bound the data; it is the onset or threshold for the enhancement that is predicted nonconservatively. In terms of K_{max}, as noted previously at rise times between 12 and 60 s, the threshold is predicted conservatively by ≈5 MPa·m$^{1/2}$. For much longer rise times, the predicted value of the threshold K_{max} is nonconservative by ≈12 MPa·m$^{1/2}$. Most of the data upon which the correlation for the EAC threshold is based were obtained for rise times of ≈10–60 s; consequently extrapolation to longer rise times may be inaccurate, or the nonconservative prediction of CGRs may be caused by the nickel-chromium plating on the specimen. Further testing is needed to resolve the issue.

Direct comparison of the behavior of plated or Inconel-182 clad specimens and with nonplated specimens suggests that plated or weld-clad specimens are more susceptible to cracking. When loaded in series and tested under identical conditions, cracks initiate first in clad specimens and tend to propagate under a wide range of loading conditions.[23,24] However, the CGRs, except for tests with very long rise times, seem to be predicted reasonably well by the crack growth correlations proposed for inclusion in Section XI of the ASME code.

At the end of the first series of tests, specimen 02C-07 was sectioned for metallographic examination. The specimen was etched with 2% Nital for 20 seconds. A cross-sectional view of the entire crack and a photomicrograph of the crack tip region are shown in Figs. 12(A) and (B), respectively. The overall crack plane is straight; however, some local branching of <20 μm is also visible in Fig. 12(A). Figures 12(C) and (D) are SEM photographs of the crack surface and the tensile fracture surface produced in air atmosphere at room temperature. The crack surface exhibits a transgranular mode of crack growth, whereas the tensile fracture surface shows predominantly microvoid coalescence.

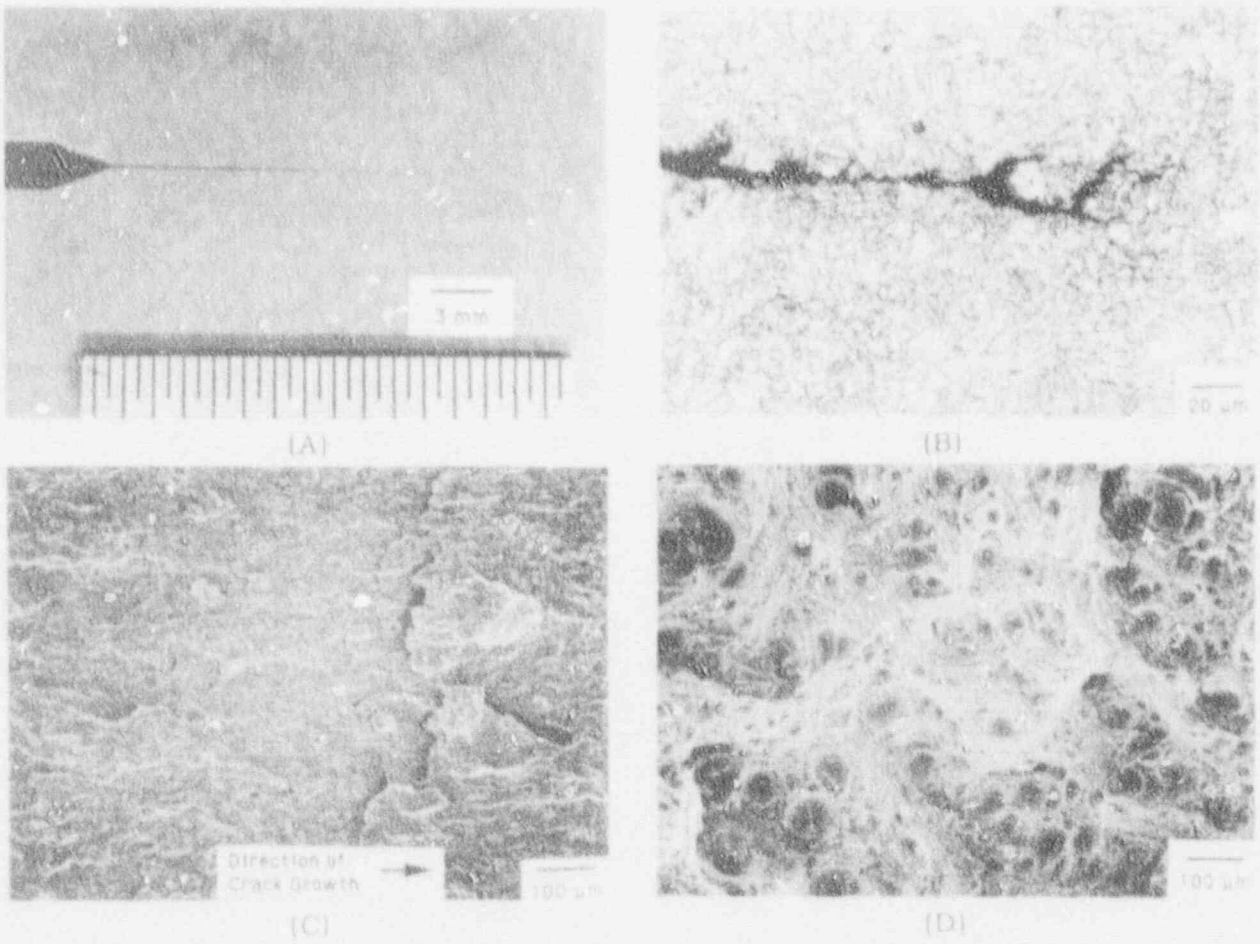

Figure 12. Cross-section and SEM micrographs of Cr-Ni plated A533-Gr B specimen 02C-07. (A) crack path, (B) crack-tip region, (C) crack surface showing transgranular crack growth in high-purity oxygenated water at 289°C, and (D) tensile fracture surface produced in air at room temperature

4 Irradiation-Assisted Stress Corrosion Cracking of Austenitic SS

In recent years, failures of reactor-core internal components in both BWRs and PWRs have increased after accumulation of relatively high fluence (>5 x 10^{20} n·cm^{-2}, E >1 MeV). The general pattern of the observed failures indicates that as nuclear plants age and neutron fluence increases, various apparently nonsensitized austenitic materials become susceptible to intergranular failure. Some components are known to have cracked under minimal applied stress. Although most failed components can be replaced, some safety-significant structural components, such as the BWR top guide, shroud, and core plate, would be very difficult or impractical to replace. Therefore, the structural integrity of these components after accumulation of high fluence has been a subject of concern, and extensive research has been conducted to provide an understanding of this type of degradation, which is commonly known as irradiation-assisted stress corrosion cracking (IASCC).[25–42]

Most of the safety-significant structural components are fabricated from solution-annealed austenitic SSs, primarily commercial-purity Type 304 SS. Component fabrication procedures and reactor operational parameters, such as neutron flux, fluence, temperature, water chemistry, residual stress, and mechanical loads, have been reported to influence susceptibility to IASCC.[25–36] However, results from different laboratories on materials irradiated under a wide variety of simulated conditions are often inconsistent and conflicting as to the influence of these parameters.[28,35]

Failures of austenitic SS after accumulation of high fluence have been attributed to irradiation-induced segregation (RIS) or depletion of elements such as Si, P, S, Ni, and Cr at grain boundaries. It is generally believed that the nonequilibrium process of RIS of impurity or alloying elements is strongly influenced by irradiation temperature and fast-neutron dose rate. However, the exact identity of the elements that segregate and the extent to which RIS contributes to the enhanced susceptibility of the core-internal components of LWRs to IASCC are not clear. This is particularly true for Type 304 SS, from which the majority of the safety-significant in-core components have been fabricated, although analyses of RIS of impurity elements and grain-boundary depletion of Cr have been reported for Type 304 SS specimens irradiated under simulated conditions, i.e., either in test reactors[29,30,32] or by electrons[29] or ions.[34,36]

In view of the strong influence of irradiation temperature and dose rate, results obtained from specimens irradiated in test reactors and accelerators must be considered as tentative, and benchmark analyses on actual reactor components must be obtained. For this purpose, high- and commercial-purity (HP and CP) Type 304 SS specimens obtained from neutron-absorber tubes of two operating BWRs were analyzed previously by Auger electron spectroscopy (AES), and susceptibility to SCC was determined from slow-strain-rate-tensile (SSRT) tests.[40–42] HP Type 304 SS has been suggested as an alternative to CP Type 304 SS. In-reactor and laboratory experience[26,27,33] indicate better IASCC performance of an HP heat of Type 348 SS than of a CP heat of Type 348 SS. However, superior resistance to IASCC of HP heat of Type 304 SS has not been established,[42] although there is an indication of relatively better performance of HP neutron-absorber rods in an in-reactor noncrevice environment.* Preliminary results obtained from

* A. J. Jacobs, General Electric Company, San Jose, CA; private communication, February 1992.

laboratory SSRT tests on irradiated specimens in simulated BWR water indicated an opposite trend.[42]

In the present study, specimens obtained from absorber tubes fabricated from two additional heats of HP Type 304 SS and from a control-blade sheath fabricated from one additional heat of CP Type 304 SS were analyzed by Auger electron spectroscopy. SSRT tests were also conducted on specimens obtained from the CP control-blade sheath, and the results were compared with similar data obtained from HP absorber tubes.

4.1 Slow-Strain-Rate Tests on Irradiated Austenitic SS (H. M. Chung, W. E. Ruther, and A. Purohit)

4.1.1 Experimental Methods

Specimen preparation and procedures for preparation of the SSRT test specimens and a description of the hot-cell SSRT apparatus were given in previous reports.[41,42] Cylindrical SSRT specimens (89 mm long) were sectioned from top-, middle-, and bottom-axial positions of the neutron-absorber rods, and boron carbide was removed with diamond-tip drills. Maximum fluence at the top was determined from known in-reactor flux data. Lower fluences at the other two axial locations were determined from results of ^{60}Co gamma scans on the entire length of the rods. Sheet tensile specimens 57.2-mm-long, 12.7-mm-wide, and 1.22-mm-thick were fabricated from a control-blade sheath irradiated in BWR-LC. The length and width of the gage section were ≈19 and 3.2 mm, respectively. The material was obtained from the General Electric Co. Vallecitos Nuclear Center. The fast-neutron fluence and chemical composition of all HP and CP Type 304 SS neutron-absorber tubes and the control-blade sheath are given in Table 4. Documents on the chemical composition of the as-fabricated neutron-absorber and control-blade sheath of the CP-grade steels were not available from either the utility or the reactor-fuel supplier. Compositions of the three HP heats are similar except for the nitrogen content. Absorber-tube specimens fabricated from HP Heat-CD, which was irradiated in BWR-QC (Component Code QC-AT), have been examined as part of the round-robin study of the International Cooperative Group on Irradiation-Assisted Stress Corrosion Cracking (ICG-IASCC).

SSRT tests were conducted on eight specimens of the CP control-blade sheath in air and in simulated BWR water at 289°C at a strain rate of 1.65×10^{-7} s^{-1} to determine tensile properties and IASCC susceptibility as a function of neutron fluence. The dissolved-oxygen concentration and conductivity of the simulated BWR water were ≈310 ppb and 0.12 $\mu S \cdot cm^{-1}$, respectively. The fracture surface of the SSRT specimens was evaluated by SEM and the chemical composition of precipitates was analyzed by energy-dispersive X-ray spectroscopy (EDS). The SEM fractography was conducted at magnifications of 60 to 800X, and an entire fracture-surface composite was constructed for each specimen to determine the fraction of intergranular(IG), transgranular (TG), and ductile failure.

4.1.2 Results

4.1.2.1 Tensile Properties

Test conditions, SSRT data, and SEM analyses of the HP and CP absorber-tube specimens are summarized in Table 5. Similar data for the eight sheath specimens are given in Table 6. Stress versus elongation curves for the CP sheath specimens obtained during this reporting period are shown in Fig. 13. The figures portray SSRT data for high-, medium-, and low-fluence sheath specimens strained to failure in simulated BWR water and air. Similar plots obtained for the HP and CP absorber tubes listed in Table 5 were reported previously.[42] The relative characteristics of stress corrosion of the sheath specimens can be deduced from Fig. 13. As fluence increases, the ratio of elongation in water to that in air becomes smaller, indicating a greater degree of SCC.

Table 4. Chemical Composition and Fast-Neutron Fluence of Irradiated Type 304 SS BWR Neutron Absorber-Rod Tubes and Control-Blade Sheath

Material and Heat	Composition, wt.%										Component Code	Service Reactor	Fluence Level, 10^{21} n·cm^{-2}
	Cr	Ni	Mn	C	N	Ti	Si	P	S	O			
HP304-A	18.50	9.45	1.53	0.018	0.100	<0.01	≤0.03	0.005	0.003	–	V-AT[a]	BWR-B	0.2-1.4
HP304-B	18.70	9.75	1.32	0.015	0.080	<0.001	0.05	0.005	0.005	–	V-AT[a]	BWR-B	0.2-1.4
HP304-CD	18.58	9.44	1.22	0.017	0.037	0.001	0.02	0.0022	0.003	–	V-AT[a]	BWR-B	0.2-1.4
											QC-AT[b]	BWR-QC	2.0
CP304-A	18.86	8.77	1.65	0.06[c]	0.052	–	–	1.35	0.048[c]	0.030[c]	0.024	BL-AT[d]	BWR-Y	0.2-2.0
CP304-B	18.0-20.0	8.10-13	2.00[c]	0.08[c]	–	–	–	1.00[c]	0.045[c]	0.030[c]	–	C-S[e]	BWR-LC	0.5-2.6

[a]High-purity (HP) neutron-absorber tubes, OD = 4.78 mm, wall thickness = 0.63 mm, composition measured before service.

[b]High-purity neutron-absorber tubes, OD = 4.78 mm, wall thickness = 0.63 mm, composition measured before service.

[c]Represents maximum value in the specification; actual value not measured.

[d]Commercial-purity (CP) neutron-absorber tubes, OD = 4.78 mm, wall thickness = 0.79 mm, composition measured after service.

[e]Commercial-purity control blade sheath, thickness 1.22 mm, actual composition not measured.

Figures 14 and 15 show comparisons of the yield strength (YS) and ultimate tensile strength (UTS) versus fast-neutron fluence (E >1 MeV) of the CP and HP neutron-absorber tubes and control-blade sheath strained to failure in air (from Tables 5 and 6). The figures contain similar data for CP-grade tensile specimens of Types 304, 304L, 316L, and 316NG SS irradiated in the Advanced Test Reactor (ATR) at 300°C and reported by Jacobs et al.[30] Both the yield and ultimate tensile strengths of the high-fluence CP-grade BWR sheath are significantly higher than those of the ATR-irradiated specimens, or of the CP Type 304 SS neutron-absorber tube. The tensile strength of the CP sheath specimens is similar to that of the HP neutron-absorber tubes at a comparable fluence. While the strength of the ATR-irradiated materials tends to reach saturation at fluence ≥2.5 x 10^{21} n·cm^{-2}, the strength of BWR components seem to reach saturation at a significantly higher fluence.

Figure 16 shows the total elongation versus fast-neutron fluence for the HP and CP Type 304 SS neutron-absorber tubes and control-blade sheath. For comparison, similar data from Ref. 30 for CP heats of Types 304, 304L, 316L, and 316NG SS are also shown in

Table 5. SSRT Test[a] Results on CP and HP Type 304 SS BWR Neutron-Absorber-Rod Tubes in Air and in High-Purity Water Containing ≈280 ppb Dissolved Oxygen at 289°C

Specimen Ident. No.	Hot-cell Ident. No.	Source Heat Ident. No.	Fast-Neutron Fluence, $n \cdot cm^{-2}$	SSRT No.	Feedwater Chemistry: Oxygen Conc., ppb	Feedwater Chemistry: Cond. at 25°C, $\mu S \cdot cm^{-1}$	Feedwater Chemistry: pH at 25°C	SSRT Parameters: Failure Time, h	SSRT Parameters: Max. Stress, MPa	SSRT Parameters: Total Elong., %	SSRT Parameters: TGSCC, %	SSRT Parameters: IGSCC, %
BL-BWR-2H	389E3A	CP304-A	2.0×10^{21}	IR-9	b	b	b	228	631	13.5	0	0
BL-BWR-2H	389E3D	CP304-A	2.0×10^{21}	IR-12	300	0.13	6.27	21	415	1.2	8	28
BL-BWR-2M	389E2D	CP304-A	0.6×10^{21}	IR-3	b	b	b	580	465	34.8	0	0
BL-BWR-2M	389E2A	CP304-A	0.6×10^{21}	IR-8	290	0.15	6.32	140	359	8.3	55	0
BL-BWR-2L	389E1A	CP304-A	0.2×10^{21}	IR-2	b	b	b	260	390	15.6	0	0
BL-BWR-2L	389E1D	CP304-A	0.2×10^{21}	IR-1	280	0.13	6.23	107	337	6.7	43	0
VH-A7A-L2	406A1F	HP304-A	1.4×10^{21}	IR-5	b	b	b	93	786	5.6	0	0
VH-A7A-L1	406A1E	HP304-A	1.4×10^{21}	IR-4	280	0.10	6.28	11	417	0.6	2	58
VM-D5B-L2	406C3	HP304-CD	0.7×10^{21}	IR-6	b	b	b	405	684	24.2	0	0
VM-D5B-L1	406C2	HP304-CD	0.7×10^{21}	IR-7	280	0.12	6.26	31	552	1.8	8	34
VL-A4C-L2	406B3	HP304-A	0.2×10^{21}	IR-10	b	b	b	231	607	13.7	0	0
VL-A4C-L1	406B2	HP304-A	0.2×10^{21}	IR-11	330	0.14	6.33	77	520	4.6	47	14

[a]Strain rate of $1.65 \times 10^{-7}\ s^{-1}$.

[b]Test in air at 289°C and the strain rate of $1.65 \times 10^{-7}\ s^{-1}$.

Table 6. SSRT Test[a] Results on CP Type 304 SS BWR Control-Blade Sheath[b] in Air and in High-Purity Water Containing ≈280 ppb Dissolved Oxygen at 289°C

Control-Blade Sheath Specimen No.	Hot-Cell Identification No.	Fast-Neutron Fluence, $n \cdot cm^{-2}$	SSRT No.	Feedwater Chemistry: Oxygen Conc., ppb	Feedwater Chemistry: Cond. at 25°C, $\mu S \cdot cm^{-1}$	Feedwater Chemistry: pH at 25°C	SSRT Parameters: Failure Time, h	SSRT Parameters: Maximum Stress, MPa	SSRT Parameters: Total Elong., %	SSRT Parameters: TGSCC, %	SSRT Parameters: IGSCC, %
C71U	LSC-1	2.45×10^{21}	IR-15	c	c	c	123	830	7.3	–	–
C71X	LSC-2	2.26×10^{21}	IR-16	310	0.12	6.23	74	841	4.2	2	3
C72T	LCS-4	2.54×10^{21}	IR-13	c	c	c	121	876	7.2	–	–
C72S	LCS-3	2.64×10^{21}	IR-14	320	0.11	6.25	84	843	5.0	2	4
C7T1T	LSC-7	1.59×10^{21}	IR-19	c	c	c	203	792	15.0	–	–
C7T1J	LCS-8	1.53×10^{21}	IR-20	360	0.11	6.22	101	872	6.1	3	6
C7B1W	LCS-5	0.23×10^{21}	IR-17	c	c	c	574	577	34.1	–	–
C7B1X	LSC-6	0.20×10^{21}	IR-18	310	0.11	6.24	457	572	27.1	8	0

[a]Strain rate of $1.65 \times 10^{-7}\ s^{-1}$.

[b]Source heat CP304-B.

[c]Test in air at 289°C and strain rate of $1.65 \times 10^{-7}\ s^{-1}$.

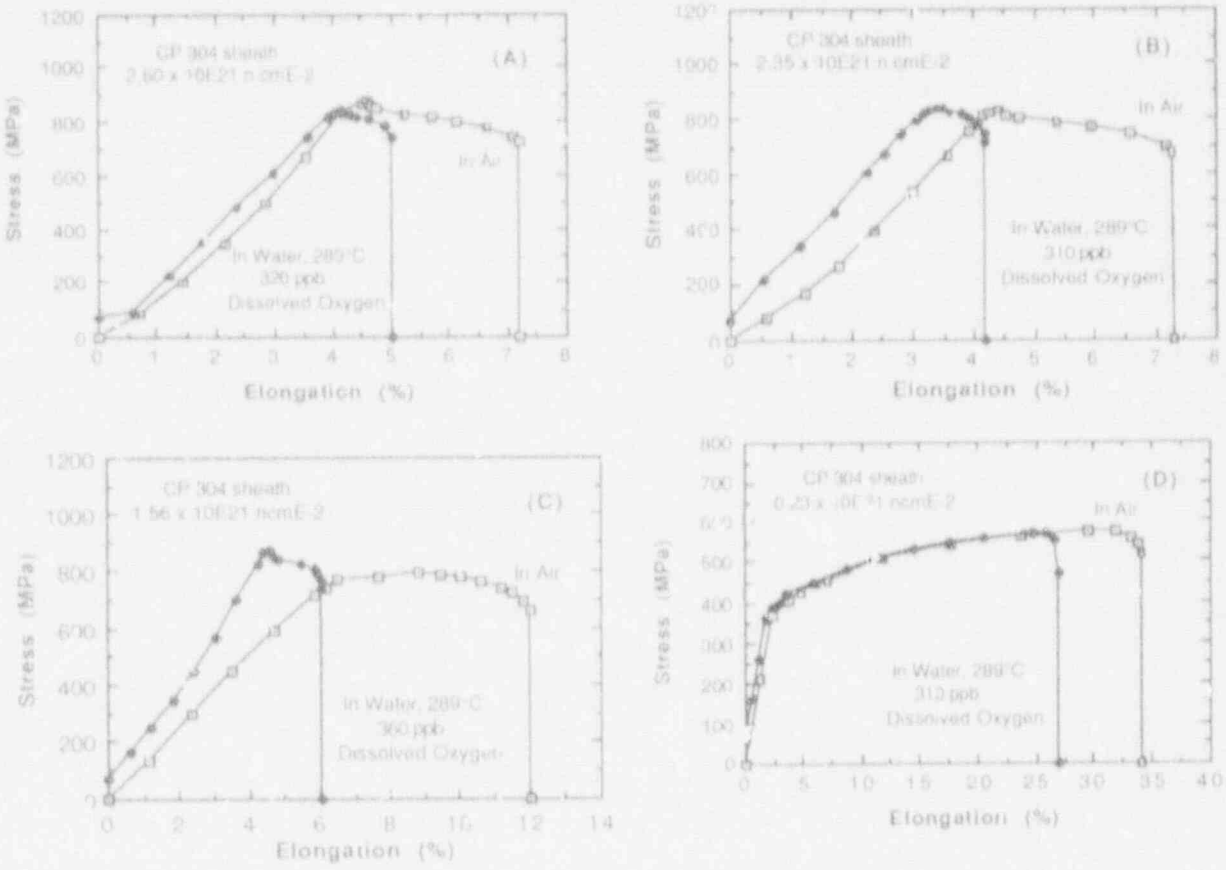

Figure 13. Stress vs. elongation from SSRT tests in air and in simulated BWR water at 289°C on CP Type 304 SS BWR control-blade sheath irradiated to a fluence of (A) 2.60 x 10^{21}; (B) 2.35 x 10^{21}; (C) 1.59 x 10^{21}; and (D) 0.23 x 10^{21} n·cm^{-2}

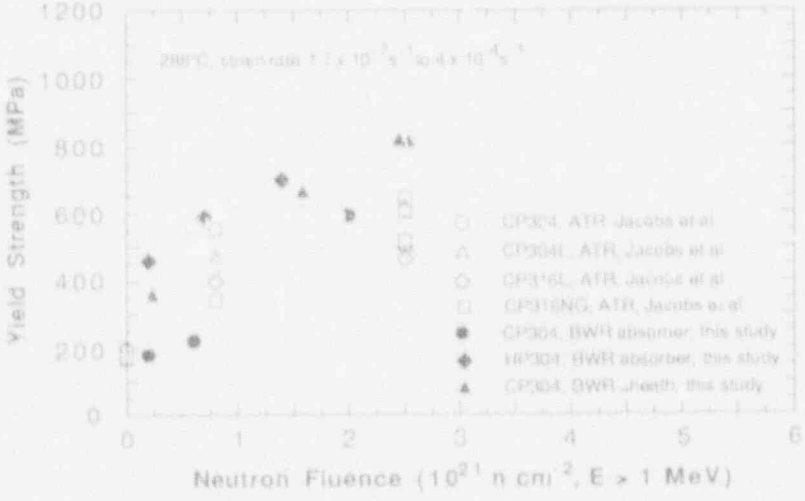

Figure 14. Yield stress vs. fast neutron fluence (E >1 MeV) for solution-annealed CP and HP Type 304 and 316 SS from tensile tests in air at 289°C.

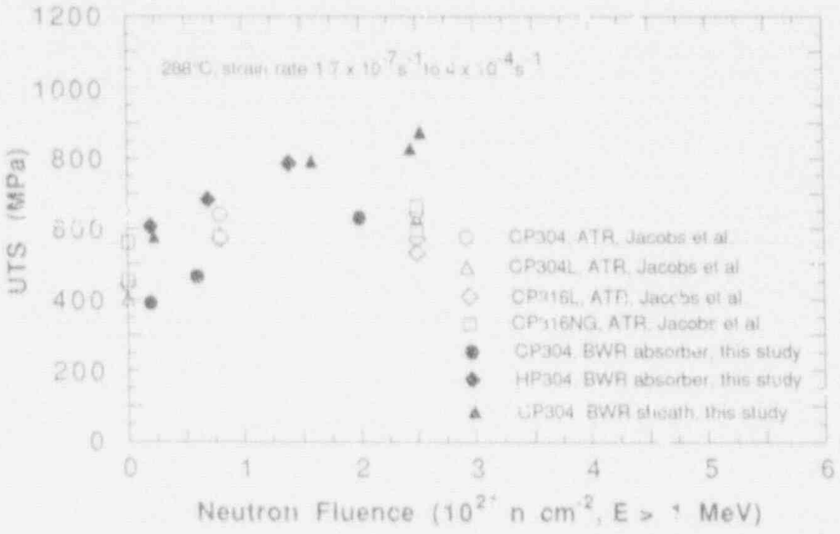

Figure 15. Ultimate tensile stress (UTS) vs. fast-neutron fluence (E >1 MeV) for solution-annealed CP and HP Types 304 and 316 SS from tensile tests in air at 289°C

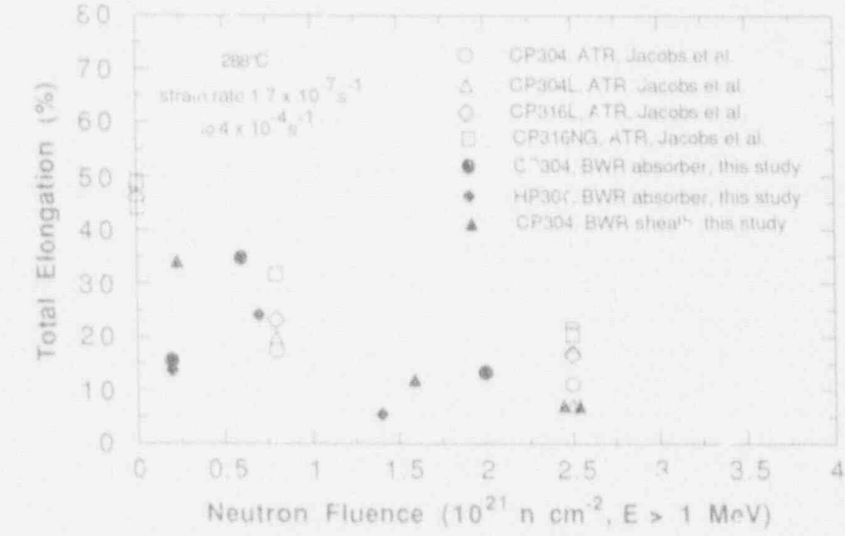

Figure 16. Total elongation vs. fast-neutron fluence (E >1 MeV) for solution-annealed CP and HP Types 304 and 316 SS from tensile tests in air at 289°C

the figure. The latter data were obtained at a significantly higher strain rate than that in the present tensile tests, i.e., 4 x 10^{-4} s^{-1} versus 1.7 x 10^{-7} s^{-1}. Despite differences in strain rate and composition (i.e., HP vs. CP), the effects of fluence on total elongation of both heats seem to be essentially similar considering the significant scatter in the data. Ductility appears to reach an asymptotic minimum value of ≈5% at fluence levels >1.5 x 10^{21} n/cm^{-2}. The total elongations of the BWR-irradiated materials are, however,

considerably smaller than those of the ATR-irradiated materials at the high fluence level, i.e., 5-10 vs. 8-22 %.

4.2.2 SCC Susceptibility

The ratio of total elongation in simulated BWR water and in air (Fig. 13) gives an indication of SCC susceptibility of the CP sheath specimens. In comparison with similar ratios obtained for CP and HP neutron-absorber tubes reported previously,[42] the ratio for the CP sheath was significantly smaller for a comparable fluence level, indicating significantly lower SCC susceptibility for the CP sheath material than for the HP and CP absorber tubes.

To determine SCC susceptibilities more quantitatively, SEM micrographs of the fracture surfaces of the absorber tube and sheath specimens were obtained. The fractions of IG and TG fracture, i.e., percent IGSCC and TGSCC, respectively, were measured from composite fracture surface maps and the results are given in Tables 5 and 6, respectively. The amount of IGSCC for CP sheath specimens irradiated to a fluence of $\approx 2.5 \times 10^{21}$ n·cm^{-2} was only 3-4% (Table 6). This is significantly lower than that of the CP absorber tube (Table 5). An example of IG fracture-surface morphologies for sheath specimens irradiated to $\approx 3.5 \times 10^{21}$ n·cm^{-2} is shown in Fig. 17. IGSCC in the corner of the fracture surface, surrounded by TGSCC, corresponds to only ≈3%.

For HP and CP specimens tested in simulated BWR water, the percent IGSCC determined from SEM fractography was, in general, consistent either with total elongation or with the ratio of elongation in water and in air. This is shown in Figs. 18 and 19, respectively. Total elongation values were corrected (increased) to account for the initial elongation caused by the stress exerted on the specimens in high-pressure water before the mechanical load was applied. The correction was negligible in SSRT tests of the sheath specimens. Literature data from SSRT tests on Types 304 and 316 SS from CP-grade BWR components are also plotted in Fig. 18. These figures indicate that either total elongation or the elongation ratio (water/air) is a good measure of IGSCC susceptibility. However, IGSCC susceptibility could not be correlated well with the increase in yield strength (i.e., irradiated minus as-fabricated yield strength).

Figure 20 shows a relationship between the percent IGSCC and neutron fluence for our CP absorber tubes and control-blade sheath of Type 304 SS, along with similar data of Clark and Jacobs,[25] Jacobs et al.,[30] and Kodama et al.[43] on CP heats of Types 304 and 316 SS. The materials in the study by Jacobs et al.[30] were irradiated at 300°C in the ATR, whereas the other heats tested by Kodama et al.[43] were from BWR-irradiated dry tubes. SSRT tests in all of the studies were conducted at 289°C in simulated BWR water containing several dissolved-oxygen concentrations, namely, 0.2, 8, or 32 ppm. Despite the wide range of strain rates and dissolved oxygen concentrations in the various tests, the dependence of IG fracture morphology (percent IGSCC) on neutron fluence is reasonably consistent.

A comparison of the percent IGSCC versus fast-neutron fluence (E >1 MeV) for the present CP and HP neutron absorber tubes and CP control blade sheath is shown in Fig. 21, along with similar results from SSRT tests on CP grade BWR duplex tubes reported by Kodama

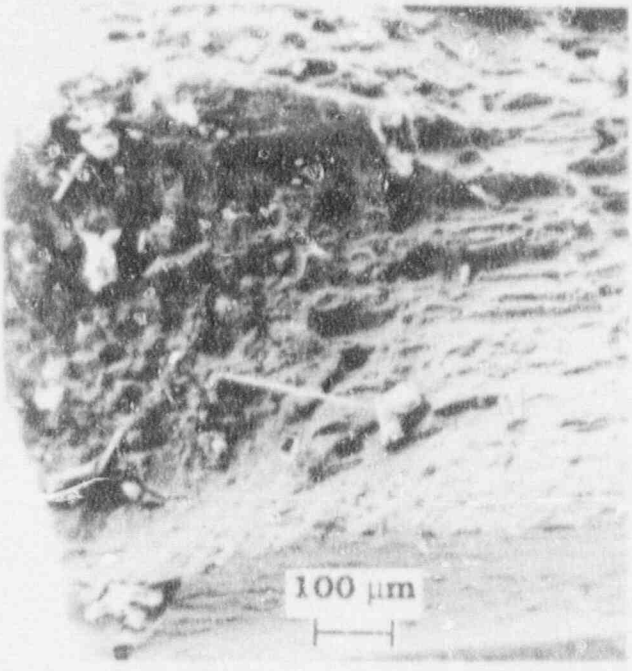

Figure 17. SEM fracture surface morphology of SSRT specimen from a CP Type 304 SS control-blade sheath irradiated to fluence of 2.26 x 10^{21} n·cm^{-2}

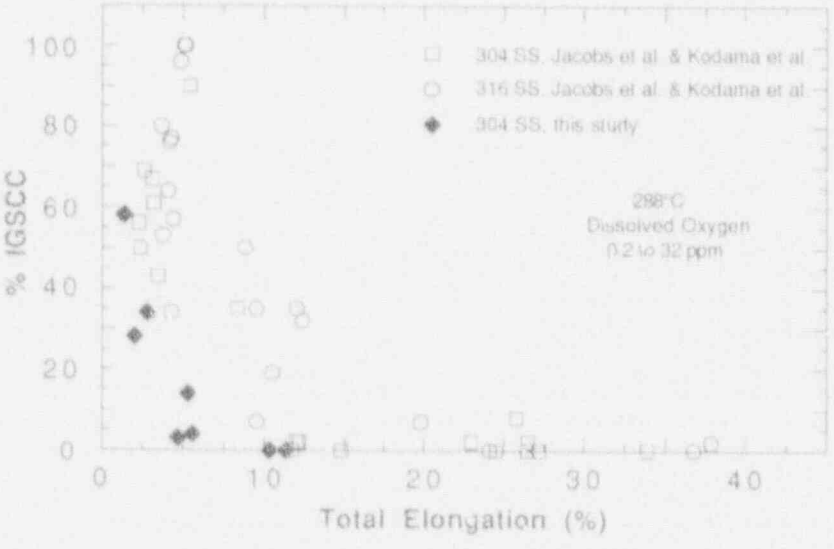

Figure 18. Percent IGSCC vs. total elongation of CP and HP Type 304 SS in the present study and similar data from the literature[30,32,33,43] from SSRT tests at 289°C in simulated BWR water containing 0.2 to 32 ppm dissolved oxygen

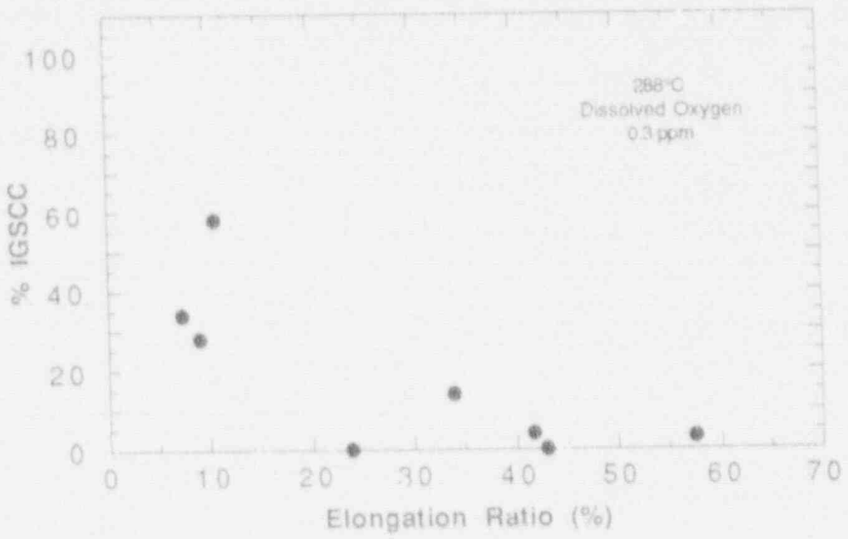

Figure 19. Percent IGSCC vs. ratio of total elongation in water and in air of CP and HP Type 304 SS in the present SSRT tests.

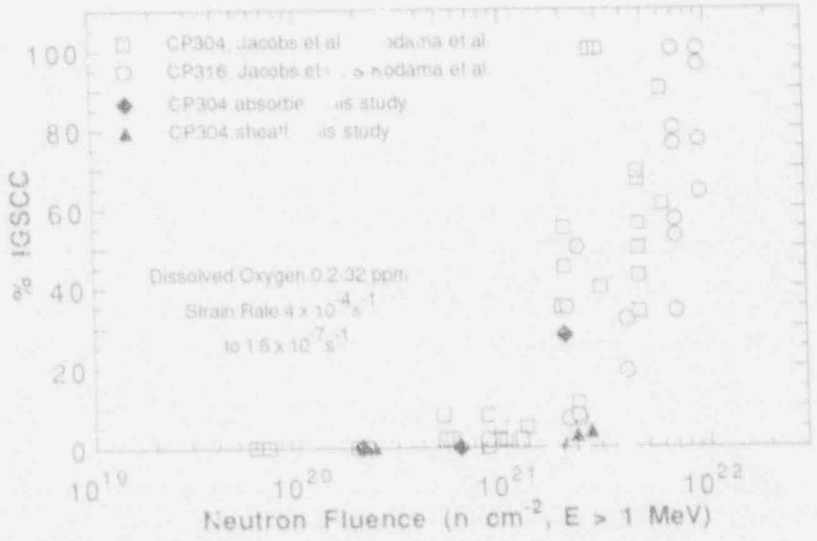

Figure 20. Percent IGSCC vs. fluence (E >1 MeV) for CP Types 304 and 316 SS from SSRT tests at 289°C in simulated BWR water containing 0.2–32 ppm dissolved oxygen

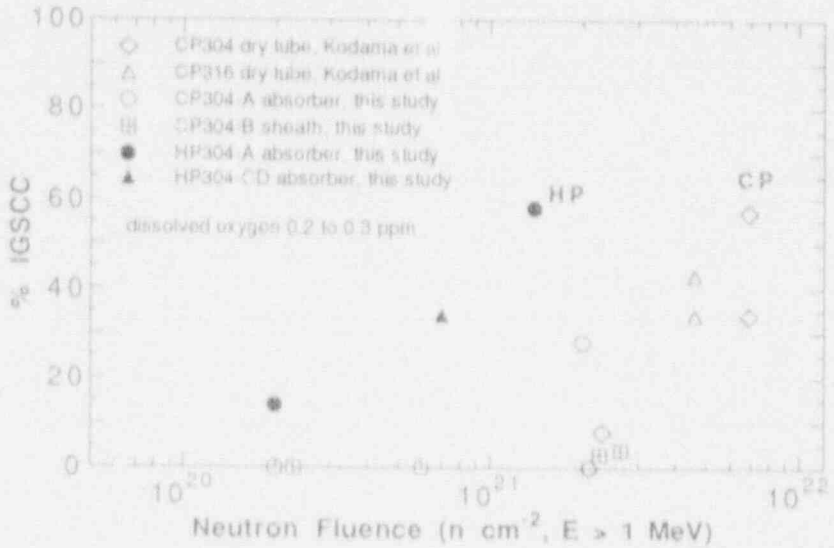

Figure 21. Percent IGSCC in SSRT tests on BWR-irradiated HP Type 304 SS and CP Types 304 and 316 SS at 289°C in water containing ≈300 ppb dissolved oxygen vs. fast-neutron fluence (E >1 MeV) of the components. HP material exhibits higher susceptibility than do CP heats.

containing ≈300 ppb dissolved oxygen. The figure indicates that IGSCC susceptibility of the CP control-blade sheath is significantly lower than that of the CP neutron-absorber tube or the dry tube of Kodama et al.[43] for a comparable fluence level. The susceptibility of the HP absorber tube is greater than that of any of the CP materials.

4.2 Auger Electron Spectroscopy Analysis of Irradiated Austenitic SS (H. M. Chung and J. E. Sanecki)

Specimens sectioned from the CP control-blade sheath irradiated in BWR-LC (Table 4) and HP neutron-absorber tube irradiated in BWR-QC were analyzed by Auger electron spectroscopy (AES) to determine grain-boundary segregation and depletion of impurities and Cr. The analyses were conducted as part of the international round-robin study. Procedures for hydrogen charging and in-situ fracture of the specimens in the ultra-high vacuum of the scanning-Auger microscope were similar to those reported previously.[41] For comparable fluence and hydrogen-charging time, it was easier to produce IG fracture in the HP absorber tube (Heat HP304-CD, Table 4) than in the HP absorber tube (Heat HP304-A) irradiated in BWR-B. Compared to other heats listed in Table 4 irradiated to a comparable high fluence of ≈2 x 10^{21} n-cm^{-2}, it was rather difficult to produce IG fracture in vacuo in absorber tubes fabricated from HP Heat HP304-A irradiated in BWR-B. This is in contrast to the relative IGSCC susceptibility from SSRT tests in simulated BWR water (Fig. 21).

4.2.1 Results

Auger signals from several spots on ductile and IG fracture regions were analyzed, and peak-to-peak amplitudes of the primary peaks of Ni, Si, P, C, N, S, and the unidentified $X_{59\text{-}eV}$ peak[41] were measured and normalized with respect to the amplitude of the primary peak of Fe. The results obtained for a CP sheath specimen (Heat CP304-B, Table 4) irradiated to a fluence of $\sim 9 \times 10^{21}$ n·cm^{-2} are given in Fig. 22. Similar results obtained for HP absorber tube (Heat HP304-CD), irradiated in BWR-QC to a fluence of $\sim 2.0 \times 10^{21}$ n·cm^{-2}, are shown in Fig. 22. The normalized amplitudes shown in the figures correspond to the relative abundance of each element on (denoted "I") and away from (denoted "D") grain boundaries, and thus grain-boundary segregation of each element can be determined from a comparison of the two groups of normalized amplitudes.

From Fig. 22, grain-boundary segregation of Ni, Si, P, and the unidentified $X_{59\text{-}eV}$ element in the CP sheath are evident. This is similar to the behavior of CP absorber tubes irradiated in BWR-B (Heat CP304-A).[41] In the present CP sheath, there is an indication of segregation of C, although the evidence is considered not conclusive and further verification is necessary (Fig. 22E). No evidence of segregation of N or S was observed either in the CP sheath or the CP absorber-tube specimens.

In distinct contrast to those of CP sheath specimen, the results in Fig. 23 show detectable but very low levels of segregation of Si or P in the HP absorber tube (Heat HP304-CD) irradiated to a fluence of $\sim 2 \times 10^{21}$ n·cm^{-2}. In previous analyses,[41] segregation of Si and P could not be detected in a similar HP absorber tube (Heat HP304-A) irradiated in BWR-B to a fluence of $\sim 1.4 \times 10^{21}$ n·cm^{-2}. In addition to the fluence level and the reactor, the two heats of HP absorber tubes differ only in N content. However, unlike Heat HP304-A, segregation of the unidentified $X_{59\text{-}eV}$ element was significant in Heat HP304-CD. It appears that this is related to the observation that IG fracture in vacuo was relatively easier to produce in the latter heat than in the former. In the HP304-CD sheath specimen, segregation of N by a factor of ~1.5-1.9 could be also detected (Fig. 23F).

The intensity of the S peak was, in general, stronger in a specimen that was fractured following the hydrogen-charging and Cu plating procedure than in a specimen fractured without the Cu plating step. Apparently, S contamination occurred during Cu plating in which an S-containing solution was used; no evidence of S segregation was observed in any specimens without Cu plating.

As pointed out previously, the distribution of Cr near a grain boundary could be characterized only by the sputter depth-profile technique.[41,44] A Cr-depletion profile obtained from a specimen of the CP control-blade sheath is shown in Fig. 24. In the figure, a similar result obtained from the HP absorber tube (fabricated from Heat HP304-CD and irradiated in BWR-QC) is also shown for comparison. Cr depletion is more pronounced in the HP absorber tube (depletion ratio ~0.42) than in the CP sheath (depletion ratio 0.85) for a comparable fluence level. This is consistent with results reported previously.[41,44] Based on Cr-depletion profiles analogous to those in Fig. 24, minimum Cr contents on grain boundaries of the CP and HP absorber tubes[41,43] and the control-blade sheath were estimated and are summarized in Table 7.

Figure 22. Normalized amplitudes of (a) Ni; (b) Si; (c) P; (d) an unidentified element (denoted $X_{59.4eV}$); (e) C; (f) N; and (g) S that were obtained from ductile- (denoted by letter D) and intergranular- (I) fracture surfaces of CP Heat 304-B irradiated in BWR-LC to fluence of ~2.0 x 10^{21} n·cm^{-2} (E >1 MeV)

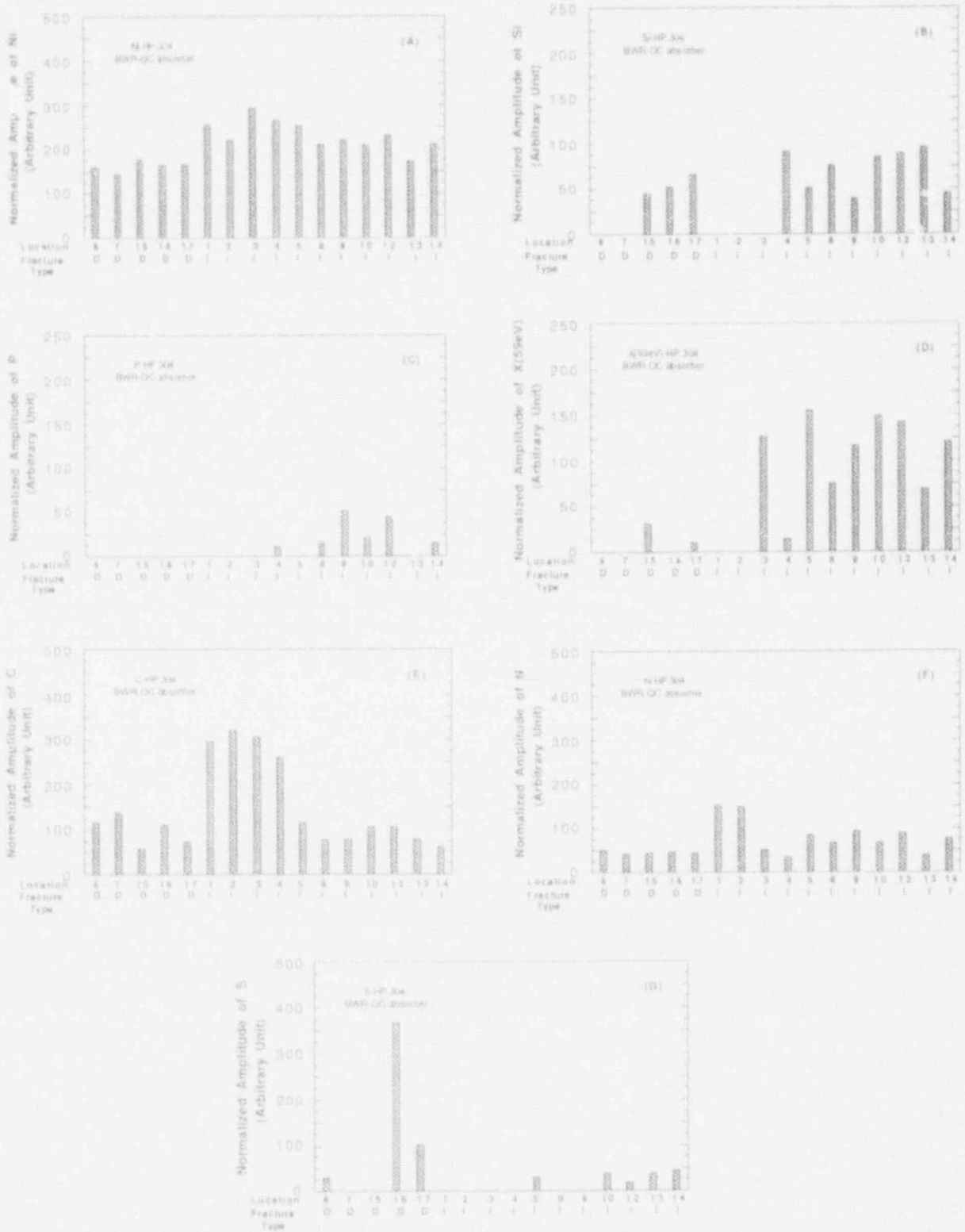

Figure 23. Normalized amplitudes of (a) Ni; (b) Si; (c) P; (d) an unidentified element (denoted $X_{5.9\ eV}$); (e) C; (f) N; and (g) S that were obtained from ductile- (denoted by letter D) and intergranular- (I) fracture surfaces of HP Heat 304-CD irradiated in BWR-QC to fluence of ≈2.0 x 10^{21} n·cm^{-2} (E >1 MeV)

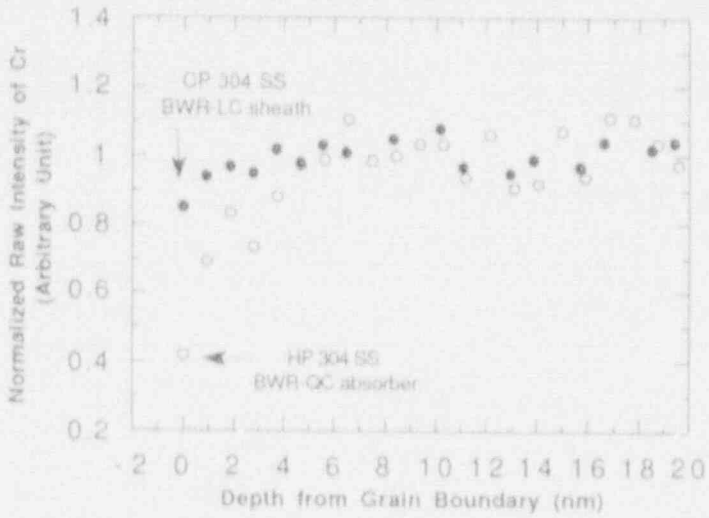

Figure 24. Comparison of grain-boundary Cr-depletion profiles of CP sheath and HP absorber tube irradiated to ~2.0 x 10^{21} n·cm^{-2} (E >1 MeV) in BWR-LC and -QC, respectively

Table 7. Summary of Minimum Grain-Boundary Cr Levels of High- and Commercial-Purity Type 304 SS BWR Components Determined by AES Depth-Profile Technique

Material and Heat	Component Code	Service Reactor	Fluence, 10^{21} n·cm^{-2}	Minimum Cr Content, wt.%
HP304 -A	V-AT[a]	BWR-B	1.4	7.9-9.3
HP304-B	V-AT[a]	BWR-B	–	–
HP304-CD	V-AT[a]	BWR-B	–	–
	QC-AT[a]	BWR-QC	? 0	7.8
CP304 -A	BL-AT[b]	BWR-Y	2.0	12.8-14.8
CP304 -B	LC-S[c]	BWR-LC	2.0	15.9

[a]High-purity (HP) neutron-absorber tubes, OD = 4.78 mm, wall thickness = 0.63 mm.

[b]Commercial-purity (CP) neutron-absorber tubes, OD = 4.78 mm, wall thickness = 0.79 mm.

[c]CP control-blade sheath, thickness = 1.22 mm.

It is difficult to explain the high percentage of IG fracture in the HP absorber-tube specimens of Heat HP304-A on the basis of Si or P segregation because impurity segregation in the HP heat was negligible. Also despite the significant Si or P segregation present in these materials, the CP-sheath specimens showed negligible SCC susceptibility. Therefore, it seems that grain-boundary segregation of Si or P cannot be the mechanism of IASCC, as has often been suggested.

At least in simulated BWR water, the results of the SSRT tests of the CP and HP components seem to be consistent with a mechanism in which irradiation-induced Cr depletion is the primary process. This is shown in Fig. 25 in which percent IGSCC and minimum grain-boundary Cr levels of one HP heat (HP304-A) and two CP heats (CP304-A and -B) have been plotted. Although the data are limited, the results are similar to those reported by Bruemmer et al.[45] In their study, SSRT tests were conducted on Type 304 SS specimens in which grain-boundary Cr depletion was produced by thermal sensitization. The Cr depletion was compared to that produced by ion irradiation at 500°C. Because of the high temperature during irradiation, the Cr-depletion profiles were significantly wider than in the present BWR components, and measurement of a minimum Cr content by scanning-transmission-electron microscopy (STEM) was somewhat easier. For extremely narrow Cr-depletion profiles, such as those in the present BWR components, it would be difficult to determine the true minimum in Cr content by STEM examination with similar resolution. For comparable levels of minimum Cr concentration, the narrower width of Cr depletion in the present BWR components is expected to produce a lower SCC susceptibility. The relatively higher SCC susceptibility of the HP Type 304 SS BWR components observed from the present laboratory SSRT tests is also consistent with results obtained recently from SSRT tests on proton-[46] and ion-irradiated[47] HP and CP Type 304 SS. However, explanations for the somewhat higher SCC susceptibility of proton- and ion-irradiated HP materials have been not reported.

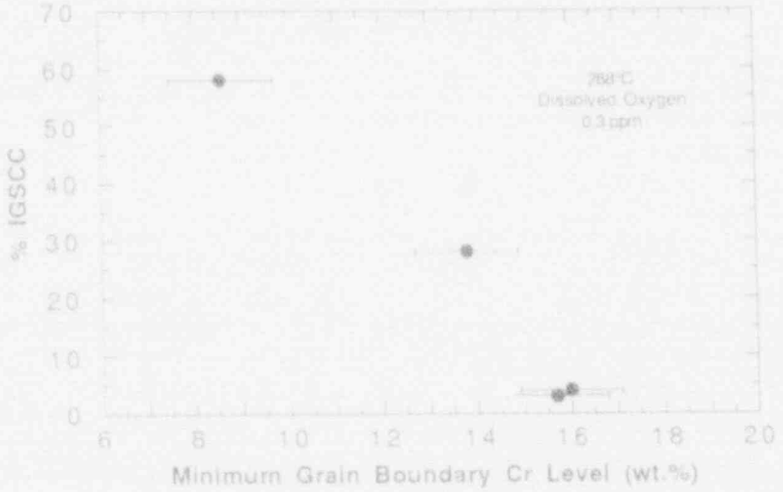

Figure 25. Percent IGSCC from SSRT tests vs. minimum grain-boundary Cr content from AES analysis of HP and CP Type 304 SS BWR components

5 Crack Growth Data Base for Austenitic and Ferritic Steels

The objective of this work is to evaluate the resistance of austenitic and ferritic steels to environmentaly assisted cracking in simulated BWR water. Alternative materials for recirculation system piping in BWRs, e.g., Types 316NG and 347 SS, are very resistant to sensitization and thus are much less susceptible to IGSCC than Types 304 and 316 SS used

in many operating reactors in the U.S. However, these steels can undergo other modes of degradation, such as TGSCC and corrosion-assisted fatigue, in simulated reactor water chemistries.[48] Plain carbon steels are used extensively in PWR and BWR nuclear steam supply systems as piping and pressure vessel materials. The steels of interest for these applications include A106-Gr B and A333-Gr 6 for seamless pipe and A302-Gr B, A508-2, and A533-Gr B plate for pressure vessels. Although operating experience with ferritic steel components in reactor pressure boundaries is considerably better than with weld-sensitized austenitic stainless steels, instances of cracking of these steels have occurred in plants in the U.S. and abroad. Ferritic steels become susceptible to TGSCC in high-temperature water containing dissolved oxygen and some evidence suggests a synergistic effect between oxygen and soluble copper compounds (viz., $CuCl_2$), as well as other impurities, to produce susceptibility to SCC. Crack growth tests have been conducted on fracture-mechanics specimens to characterize the environmental, loading, and material conditions that can produce SCC susceptibility in these steels. Data that have been obtained over the past eight years (October 1983 to September 1991) are summarized along with references that contain details of the test methods, composition of the materials, metallographic and fractographic information, and comparisons of the data with predictions based on Section XI of the ASME Code.

5.1 Summary of Crack Growth Data for Austenitic SS
(W. E. Ruther, T. F. Kassner, and J. Y. Park)

Table 8 summarizes crack growth results for Type 316NG SS and sensitized (EPR = 2, 8, 20, and 30 C-cm^{-2}) and solution-annealed Type 304 SS in high-purity water containing ≈200 ppb dissolved oxygen at 289°C. Most of the data were obtained under high-R (0.8-0.95), low-frequency (8×10^{-2} Hz) loading conditions at maximum stress intensity values of 27-46 MPa·m$^{1/2}$. Table 9 contains data on sensitized and solution-annealed Type 304 SS in high-purity water containing 5-8 ppm dissolved oxygen at 289°C over a wider range of load ratio, frequency, and stress intensity. Crack growth results for Type 316NG and sensitized and solution-annealed Type 304 SS at 289°C in water containing ≈200 ppb dissolved oxygen and ionic impurities (namely, SO_4^{2-}, CrO_4^{2-}, NO_3^-, and carboxylic acids) are summarized in Table 10. Most of the data were obtained at a load ratio of 0.95 and a frequency of 8×10^{-2} Hz. The influence of several impurity species at concentrations of ≈6-1000 ppb (conductivity values ≈0.2-3.7 μS·cm^{-1}) on CGRs of the two steels can be obtained form these data. The effect of degree of sensitization corresponding to EPR values of 0-30 C-cm^{-2} on CGRs of Type 304 SS can also be determined from these data. Table 11 summarizes CGR results for Type 347 SS specimens with different heat treatment conditions (slow-cooled and water quenched from the austenitizing temperature). These data were obtained in water containing ≈200 ppb dissolved oxygen and 100 ppb SO_4^{2-} at 289°C. No additional tests are planned for these steels. Tests are in progress on specimens of CF-3, CF-3M, CF-8, and CF-8M grades of cast SS in the as-received and thermally aged conditions.

Table 8. Summary of Crack Growth Results for Type 316NG and Sensitized and Solution Annealed Type 304 SS Specimens[a] in Oxygenated (≈200 ppb) Water[b] at 289°C in Which Load Ratio[c] and Stress Intensity Were Varied

	Potentials					Type 316NG SS			Type 304 SS					
Cond.,	304 SS,	Pt,	Load Ratio	Freq.,	Rise Time,	K_{max}[d],	ΔK,[e]	Rate,	K_{max}[d],	ΔK,	Rate,[e]	EPR,	Ref.	ANL Report
$\mu S \cdot cm^{-1}$	mV(SCE)			10^{-2} Hz	s	MPa $m^{1/2}$		10^{-10} m s^{-1}	MPa $m^{1/2}$		10^{-10} m s^{-1}	C cm^{-2}	No.	No.
0.11	–	–	0.95	8	12	–	–	–	27.3	1.37	1.00	0	49	83-85 IV
0.11	–	–	0.95	8	12	–	–	–	29.3	1.46	3.30	2	49	83-85 IV
0.11	–	–	0.95	8	12	–	–	–	29.9	1.50	3.00	20	49	83-85 IV
0.16	–	–	0.95	8	12	–	–	–	28.0	1.40	1.80	0	49	83-85 IV
0.16	–	–	0.95	8	12	–	–	–	30.3	1.51	0.40	2	49	83-85 IV
0.16	–	–	0.95	8	12	–	–	–	31.3	1.56	2.80	20	49	83-85 IV
0.14	–	–	0.95	8	12	–	–	–	28.4	1.42	1.60	0	49	83-85 IV
0.14	–	–	0.95	8	12	–	–	–	31.5	1.57	2.50	2	49	83-85 IV
0.14	–	–	0.95	8	12	–	–	–	31.9	1.59	2.20	20	49	83-85 IV
0.15	–	–	0.95	8	12	–	–	–	30.0	1.50	1.70	0	50	85-33
0.15	–	–	0.95	8	12	–	–	–	37.0	1.85	2.50	2	50	85-33
0.15	–	–	0.95	8	12	–	–	–	38.0	1.90	0.84	2	50	85-33
0.15	–	–	0.95	8	12	–	–	–	37.0	1.85	2.10	20	50	85-33
0.15	–	–	0.95	8	12	–	–	–	37.0	1.85	0.51	20	50	85-33
0.10	138	219	0.95	8	12	31.2	1.56	1.40	33.6	1.68	0	2	51	87-37
0.10	115	230	0.95	8	12	33.7	1.68	2.10	34.9	1.75	0	2	51	87-37
0.10	145	220	0.95	8	12	34.1	1.70	0.50	36.2	1.81	1.30	2	51	87-37
0.10	140	210	0.95	8	12	34.6	1.73	0.40	37.1	1.86	0.70	2	51	87-37
0.21	95	110	0.95	8	12	–	–	–	29.7	1.49	1.70	2	52	87-41
0.13	75	–	0.95	8	12	32.1	1.61	3.00	–	–	–	–	53	88-32
0.12	80	85	0.95	8	12	32.2	1.61	0.25	–	–	–	–	53	88-32
0.15	140	160	0.95	8	12	33.2	1.66	1.10	–	–	–	–	53	88-32
0.20	170	190	0.95	8	12	30.5	1.53	2.20	28.8	1.44	2.00	2	54	89-10
0.20	170	205	0.95	8	12	33.0	1.65	2.00	29.9	1.50	1.20	2	54	89-10
0.11	165	132	1.00	0	∞	24.5	0.00	0.27	24.5	0.00	0.53	2	55	89-40
0.19	167	190	1.00	0	∞	29.0	0.00	0.34	26.0	0.00	0.68	2	55	89-40
0.12	112	182	0.95	8	12	19.8	0.96	≈0	17.6	0.87	≈0	2	55	89-40
0.12	125	195	0.95	8	12	22.6	1.13	0.6	21.2	1.06	0.70	2	55	89-40
0.11	145	175	0.95	8	12	24.4	1.22	1.40	24.2	1.21	2.10	2	55	89-40
0.13	157	152	0.95	8	12	24.6	1.23	0.11	24.7	1.23	0.35	2	55	89-40
0.16	182	190	0.95	8	12	29.0	1.45	0.41	26.1	1.30	0.20	2	55	89-40

Table 8. Continued

Cond.,	Potentials 304 SS,	Potentials Pt,	Load Ratio	Freq.,	Rise Time,	Type 316NG SS K_{max}[d],	Type 316NG SS ΔK,[e]	Type 316NG SS Rate,	Type 304 SS K_{max}[d],	Type 304 SS ΔK,	Type 304 SS Rate,[e]	Type 304 SS EPR,	Ref.	ANL Report
μS cm^{-1}	mV(SHE)			10^{-2} Hz	s	MPa m$^{1/2}$		10^{-10} m s^{-1}	MPa m$^{1/2}$		10^{-10} m s^{-1}	C cm^{-2}	No.	No.
0.16	165	165	0.90	8	12	28.5	2.85	4.50	25.4	2.54	0.23	2	55	89-40
0.13	130	130	0.80	8	12	25.7	5.12	3.60	25.2	5.03	1.80	2	55	89-40
0.12	145	174	0.95	8	12	31.4	1.57	0.60	33.4	1.67	1.20	2	55	89-40
0.11	108	179	0.95	8	12	33.6	1.68	0.80	39.9	2.00	≈0	2	55	89-40
0.15	95	95	0.95	8	12	35.4	1.77	1.50	40.7	2.04	0.20	2	55	89-40
0.13	195	200	0.95	8	12	27.7	1.38	0.67	30.4	1.52	2.90	2	55,56	89-40,
0.12	190	200	0.95	8	12	28.9	1.45	0.90	33.6	1.68	2.90	2	55,56	&90/4
0.16	109	115	0.95	8	12	29.3	1.47	2.5	–	–	–	–	57	91/24
0.16	109	115	0.80	8	12	32.0	1.60	19.0	–	–	–	–	57	91/24
0.16	109	115	0.90	8	12	33.7	1.68	6.6	–	–	–	–	57	91/24
0.16	109	115	0.90	8	12	33.9	1.69	3.6	–	–	–	–	57	91/24
0.16	109	115	0.95	8	12	29.3	1.47	3.1	–	–	–	–	57	91/24
0.16	109	115	0.80	8	12	30.8	1.54	34.0	–	–	–	–	57	91/24
0.16	109	115	0.90	8	12	34.5	1.72	14.0	–	–	–	–	57	91/24
0.16	109	115	0.90	8	12	45.7	2.28	20.0	–	–	–	–	57	91/24
0.17	119	119	0.95	8	12	–	–	–	27.7	1.38	0.05	0	58	92/6
0.17	119	113	0.95	8	12	–	–	–	30.9	1.54	3.30	8	58	92/6
0.17	119	119	0.95	8	12	–	–	–	28.5	1.42	0.83	30	58	92/6
0.12	91	66	0.95	8	12	–	–	–	27.7	1.38	0.05	0	58	92/6
0.12	91	66	0.95	8	12	–	–	–	31.5	1.57	0.43	8	58	92/6
0.12	91	66	0.95	8	12	–	–	–	28.6	1.43	0.09	30	58	92/6

[a]Compact tension specimens (1TCT) of Type 316NG SS (Heat No. P91576) and Type 304 SS (Heat No. 30956) with the following heat treatments: solution anneal at 1050°C for 0.5 h plus 650°C for 24 h for the Type 316NG SS (EPR = 0 C cm^{-2}), and solution anneal at 1050°C for 0.5 h (EPR = 0 C cm^{-2}) followed by 700°C for 0.25 h plus 500°C for 24 h (EPR = 2 C cm^{-2}) or 700°C for 12 h (EPR = 20 C cm^{-2}) for the Type 304 SS.

[b]Effluent dissolved-oxygen concentration was 200–300 ppb; feedwater oxygen concentration was approximately a factor of 2 higher to compensate for oxygen depletion by corrosion of the autoclave systems.

[c]Positive sawtooth waveform.

[d]Stress intensity, K_{max}, value at the end of a ≈1000-h time period of steady-state crack growth.

[e]$\Delta K = K_{max}(1 - R)$, where the load ratio $R = K_{min}/K_{max}$.

Table 9. Summary of Crack Growth Results for Solution-Annealed and Sensitized Type 304 SS Specimens[a] in Oxygenated (~5–8 ppm) Water[b] at 289°C in Which Load Ratio, Frequency,[c] and Stress Intensity Were Varied

Cond., μS cm^{-1}	Potential 304 SS, mV(SHE)	Load Ratio	Freq., 10^{-2} Hz	Rise Time, s	Type 304 SS K_{max}[d], MPa m$^{1/2}$	ΔK,[e]	Rate, 10^{-10} m s^{-1}	EPR, C cm^{-2}	Ref. No.	ANL Report No.
<0.2	–	1.0	0	∞	34.0	0	1.20	1.4	59	84-60 III
<0.2	–	1.0	0	∞	37.0	0	2.90	1.4	59	84-60 III
<0.2	–	1.0	0	∞	38.0	0	4.50	1.4	59	84-60 III
<0.2	–	1.0	0	∞	33.0	0	2.20	1.8	59	84-60 III
<0.2	–	1.0	0	∞	29.0	0	1.80	HAZ	60	85-75 I
<0.2	–	0.95	8.0	12	28.0	1.40	7.50	20	61	83-85 II
<0.2	–	0.95	8.0	12	34.0	1.70	10.0	20	61	83-85 II
<0.2	–	0.95	8.0	12	35.0	1.75	12.0	20	61	83-85 II
<0.2	–	0.95	0.8	124	34.0	1.70	1.20	20	61	83-85 II
<0.2	–	0.95	0.8	124	28.0	1.90	1.50	20	61	83-85 II
<0.2	–	0.95	0.8	124	50.0	2.5[illegible]	4.70	20	61	83-85 II
<0.2	–	0.95	0.8	124	61.0	3.04	11.0	20	61	83-85 II
<0.2	–	0.95	0.8	124	64.[illegible]	3.[illegible]0	17.0	20	61	83-85 II
<0.2	–	0.95	0.08	1250	28.0	1.40	1.20	20	61	83-85 II
<0.2	–	0.95	0.08	1250	67.0	3.35	19.0	20	61	83-85 II
<0.2	–	0.95	0.08	1250	70.0	3.50	32.0	20	61	83-85 II
<0.2	–	0.95	0.08	1250	72.0	3.60	33.0	20	61	83-85 II
<0.2	–	0.95	0.2	495	36.0	1.70	1.70	1.4	59	84-60 III
<0.2	–	0.95	0.2	495	37.0	1.85	1.50	1.4	59	84-60 III
<0.2	–	0.95	0.2	495	39.0	1.95	2.00	1.4	59	84-60 III
<0.2	–	0.95	0.2	495	40.0	2.00	3.10	1.4	59	84-60 III
<0.2	–	0.95	0.2	495	28.0	1.40	2.20	HAZ	60	85-75 I
<0.2	–	0.94	10.0	5	31.0	1.86	3.10	1.4	59	84-60 III
<0.2	–	0.94	10.0	5	32.0	1.92	1.90	1.4	59	84-60 III
<0.2	–	0.94	10.0	5	30.0	1.80	2.10	1.8	59	84-60 III
<0.2	–	0.90	0.2	495	28.0	2.80	1.30	HAZ	60	85-75 I
<0.2	–	0.80	0.2	495	29.0	5.80	6.60	HAZ	60	85-75 I
<0.2	–	0.80	0.2	495	31.0	6.20	4.40	1.4	59	84-60 III
<0.2	–	0.80	0.2	495	32.0	6.3[illegible]	7.40	1.4	59	84-60 III
<0.2	–	0.70	0.2	495	32.0	6.70	5.50	1.4	59	84-60 III
<0.2	–	0.70	0.2	495	36.0	7.55	5.40	1.4	59	84-60 III
<0.2	–	0.70	0.2	495	31.0	9.30	3.40	1.4	59	84-60 III
<0.2	–	0.70	0.2	495	33.0	9.90	5.90	1.4	59	84-60 III
<0.2	–	0.60	0.2	495	29.0	11.60	56.0	1.8	59	84-60 III
<0.2	–	0.60	0.2	495	33.0	13.20	6.60	1.4	59	84-60 III
<0.2	–	0.50	0.1	995	32.0	16.00	2.60	1.4	59	84-60 III
<0.2	–	0.50	0.2	495	31.0	15.50	8.90	1.4	59	84-60 III
<0.2	–	0.50	0.2	495	33.0	16.50	34.0	1.4	59	84-60 III
<0.2	–	0.50	0.2	495	32.0	16.00	28.0	1.8	59	84-60 III

Table 9. Continued

Cond., μS·cm^{-1}	Potential, 304 SS, mV(SHE)	Load Ratio	Freq., 10^{-2} Hz	Rise Time, s	Type 304 SS: K_{max}[d], MPa·m$^{1/2}$	Type 304 SS: ΔK[e], MPa·m$^{1/2}$	Type 304 SS: Rate, 10^{-10} m·s^{-1}	Type 304 SS: EPR, C·cm^{-2}	Ref. No.	ANL Report No.
0.12	206	0.95	8.0	12	27.6	1.38	0.05	0	58	92/6
0.12	206	0.95	8.0	12	29.2	1.46	9.2	8	58	92/6
0.12	206	0.95	8.0	12	28.2	1.41	1.0	30	58	92/6

[a]Compact tension specimens (1TCT) of Type 304 SS with the following heat treatments: Heat No. 10285, solution anneal at 1050°C ± 0.5 h plus 700°C/10 min and 450°C/146 h or 450°C/250 h [EPR ≈ 1.4 C·cm^{-2}], or 500°C/24 h [EPR ≈ 1.8 C·cm^{-2}]. Heat No. 30056 solution anneal at 1050°C for 0.5 h and quenched [EPR ≈ 0 C·cm^{-2}] followed by 700°C for 0.67 h [EPR ≈ 8 C·cm^{-2}], 700°C for 12 h [EPR ≈ 20 C·cm^{-2}], or 700°C for 24 h [EPR ≈ 30 C·cm^{-2}]. HAZ specimen was fabricated from a weld overlay applied to a 12-in. diam pipe.

[b]Effluent dissolved-oxygen concentration was 5–8 ppm.

[c]Positive sawtooth waveform was used.

[d]Stress intensity, K_{max}, values at the end of a ≈500 to 1000-h time period of steady-state crack growth.

[e]$\Delta K = K_{max}(1 - R)$, where the load ratio $R = K_{min}/K_{max}$.

Table 10. Summary of Crack Growth Results for Type 316NG and Sensitized and Solution Annealed Type 304 SS Specimens[a] in Oxygenated (≈200 ppb) Water[b] with Ionic Impurities at 289°C in Which Load Ratio[c] and Stress Intensity Were Varied

Water Chemistry				Potentials		Load Ratio	Freq.,	Rise Time,	Type 316NG SS			Type 304 SS				Ref. No.	ANL Report No.
Cond., μS·cm^{-1}	SO_4^{2-}, ppb	CrO_4^{2-}, ppb	Other, ppb	304 SS, mV(SHE)	Pt.		10^{-2} Hz	s	K_{max}[d], MPa·m$^{1/2}$	ΔK,[e] MPa·m$^{1/2}$	Rate,[f] 10^{-10} m·s^{-1}	K_{max}[d], MPa·m$^{1/2}$	ΔK,[e] MPa·m$^{1/2}$	Rate,[g] 10^{-10} m·s^{-1}	EPR, C·cm^{-2}		
0.92	100	–	–	–	–	0.95	8	12	–	–	–	42.1	2.10	6.10	0	49	83-85 IV
1.04	100	–	–	–	–	0.95	8	12	–	–	–	49.8	2.49	6.90	0	49	83-85 IV
0.92	100	–	–	–	–	0.95	8	12	–	–	–	53.2	2.66	6.40	0	49	83-85 IV
1.04	100	–	–	–	–	0.95	8	12	–	–	–	63.4	3.17	16.0	0	49	83-85 IV
0.92	100	–	–	–	–	0.95	8	12	–	–	–	42.0	2.10	1.60	20	49	83-85 IV
1.04	100	–	–	–	–	0.95	8	12	–	–	–	42.2	2.11	1.00	20	49	83-85 IV
0.88	100	–	–	80	180	0.95	8	12	–	–	–	26.5	1.33	2.80	0	60	85-75 I
0.88	100	–	–	120	215	0.95	8	12	–	–	–	28.1	1.41	4.20	0	60	85-75 I
0.88	100	–	–	120	190	0.95	8	12	–	–	–	32.3	1.62	4.20	0	60	85-75 I
0.88	100	–	–	80	180	0.95	8	12	–	–	–	27.0	1.35	5.00	2	60	85-75 I
0.88	100	–	–	120	215	0.95	8	12	–	–	–	30.0	1.50	3.40	2	60	85-75 I
0.88	100	–	–	120	190	0.95	8	12	–	–	–	32.4	1.62	2.90	2	60	85-75 I
0.88	100	–	–	80	180	0.95	8	12	–	–	–	27.1	1.36	4.20	20	60	85-75 I
0.88	100	–	–	120	215	0.95	8	12	–	–	–	29.1	1.46	3.40	20	60	85-75 I
0.88	100	–	–	120	190	0.95	8	12	–	–	–	≈1.4	1.57	2.60	20	60	85-75 I
0.86	100	–	–	120	225	0.95	8	12	29.7	1.49	1.70	31.6	1.58	2.30	2	51	87-37
0.88	100	–	–	120	190	0.95	8	12	32.2	1.61	1.90	33.8	1.69	3.20	2	51	87-37
0.29	30	–	–	145	230	0.95	8	12	36.3	1.82	1.30	38.9	1.95	0.60	2	51	87-37
0.35	30	–	–	85	90	0.95	8	12	28.0	1.40	≈0	32.1	1.61	2.20	2	52	87-41
0.93	100	–	–	65	65	0.95	8	12	–	–	–	34.3	1.72	4.40	2	52	87-41
0.93	100	–	–	115	130	0.95	8	12	–	–	–	42.6	2.14	8.00	2	52	87-41
0.80	100	–	–	190	220	0.95	8	12	34.4	1.72	0.79	–	–	–	–	53	88-32
0.77	–	–	100 NO_3^-	200	215	0.95	8	12	33.7	1.68	0.84	–	–	–	–	53	88-32
0.53	50	–	–	180	180	0.95	8	12	30.0	1.50	0.86	29.9	1.5[illegible]	3.10	2	55	89-40
0.91	100	–	–	110	194	0.95	8	12	28.6	1.43	1.90	30.0	1.50	2.30	2	55	89-40
0.51	50	–	–	162	218	0.95	8	12	28.8	1.44	1.50	30.2	1.51	1.10	2	55	89-40
0.28	25	–	–	145	199	0.95	8	12	31.0	1.55	1.00	32.6	1.63	1.10	2	55	89-40
0.54	50	–	–	117	194	0.95	8	12	32.1	1.61	1.30	35.4	[illegible].77	2.80	2	55	89-40
0.94	100	–	–	138	209	0.95	8	12	33.2	1.66	1.60	39.7	1.99	2.30	2	55	89-40
0.21	–	25	–	100	179	0.95	8	12	34.6	1.73	1.70	40.6	2.03	0.20	2	55	89-40
0.51	50	–	–	162	218	0.92	8	12	30.5	2.44	4.30	32.0	2.56	4.50	2	55	89-40

Table 10. Continued

Water Chemistry				Potentials		Load		Rise	Type 316NG SS			Type 304 SS					ANL
Cond., $\mu S \cdot cm^{-1}$	SO_4^{2-}, ppb	CrO_4^{2-}, ppb	Other, ppb	304 SS, mV(SHE)	Pt, mV(SHE)	Ratio	Freq., 10^{-2} Hz	Time, s	K_{max}[d], MPa $m^{1/2}$	ΔK,[e] MPa $m^{1/2}$	Rate,[f] 10^{-10} m s^{-1}	K_{max}[d], MPa $m^{1/2}$	ΔK,[e] MPa $m^{1/2}$	Rate,[f] 10^{-10} m s^{-1}	EPR, C cm^{-2}	Ref. No.	Report No.
0.48	-	-	100 Propionic	190	190	0.95	8	12	28.0	1.40	0.64	31.4	1.57	2.90	2	58	89-40 &
3.0	-	-	1000 Propionic	206	220	0.95	8	12	28.3	1.41	0.67	31.6	1.58	0.20	2	58,59	90/4
2.5	-	-	1000 Butyric	170	180	0.95	8	12	29.2	1.46	0.64	33.6	1.68	≈0	2	58,76	〃
0.38	-	-	100 Butyric	180	190	0.95	8	12	30.2	1.51	1.20	34.8	1.74	1.90	2	58,76	〃
3.7	100	-	1000 Butyric	190	190	0.95	8	12	30.5	1.52	1.30	37.0	1.85	7.40	2	58,76	〃
3.0	-	-	1000 Butyric	190	230	0.95	8	12	30.6	1.53	0.09	37.0	1.85	≈0	2	58,76	〃
3.2	-	-	1000 Butyric + 100 Cl⁻	200	210	0.95	8	12	34.5	1.72	3.70	39.8	1.97	1.50	2	58,56	〃
3.1	-	-	1000 Butyric	175	220	0.95	8	12	35.8	1.79	4.00	39.8	1.97	≈0	2	58,56	〃
0.9	100	-	-	136	120	0.95	8	12	21.4	1.07	0.01[h]	-	-	-	-	56	90/4
0.9	100	-	-	106	66	0.25[i]	10	5	19.0	14.20	2.60[h]	-	-	-	-	56	90/4
0.9	100	-	-	81	41	0.95	8	12	21.5	1.08	0.99[h]	-	-	-	-	56	90/4
3.1	100	-	-	234	95	1.00	0	∞	21.7	0.00	0.44[h]	-	-	-	-	56	90/4
0.30	-	50	-	67	58	0.95	8	12	-	-	-	27.7	1.38	0.05	0	58	92/6
0.30	-	50	-	67	58	0.95	8	12	-	-	-	31.2	1.56	0.47	8	58	92/6
0.30	-	50	-	67	58	0.95	8	12	-	-	-	28.5	1.42	0.09	30	58	92/6
0.82	-	200	-	80	80	0.95	8	12	-	-	-	27.7	1.38	0.05	0	58	92/6
0.82	-	200	-	80	80	0.95	8	12	-	-	-	31.8	1.59	0.43	8	58	92/6
0.82	-	200	-	80	80	0.95	8	12	-	-	-	28.7	1.43	0.09	30	58	92/6
0.31	-	50	-	58	51	0.95	8	12	-	-	-	27.8	1.39	0.05	0	58	92/6
0.31	-	50	-	58	51	0.95	8	12	-	-	-	31.8	1.59	0.43	8	58	92/6
0.31	-	50	-	58	51	0.95	8	12	-	-	-	28.7	1.43	0.09	30	58	92/6
0.46	25	50	-	91	96	0.95	8	12	-	-	-	27.8	1.39	0.05	0	58	92/6
0.46	25	50	-	91	96	0.95	8	12	-	-	-	32.7	1.63	3.40	8	58	92/6
0.46	25	50	-	91	96	0.95	8	12	-	-	-	28.7	1.43	0.09	30	58	92/6
1.06	100	50	-	104	107	0.95	8	12	-	-	-	27.8	1.39	0.05	0	58	92/6
1.06	100	50	-	104	107	0.95	8	12	-	-	-	35.3	1.76	4.10	8	58	92/6
1.00	100	50	-	104	107	0.95	8	12	-	-	-	29.9	1.49	2.50	30	58	92/6
0.27	-	50	-	86	71	0.95	8	12	-	-	-	27.8	1.39	0.01	0	58	92/6
0.27	-	50	-	86	71	0.95	8	12	-	-	-	35.6	1.78	0.07	8	58	92/6
0.27	-	50	-	86	71	0.95	8	12	-	-	-	30.0	1.50	0.36	30	58	92/6
0.37	6	50	-	36	101	0.95	8	12	-	-	-	27.8	1.39	0.04	0	58	92/6
0.37	6	50	-	36	101	0.95	8	12	-	-	-	35.7	1.78	0.23	8	58	92/6
0.37	6	50	-	36	101	0.95	8	12	-	-	-	30.0	1.50	0.12	30	58	92/6

Table 10. Continued

Water Chemistry				Potentials		Load		Rise	Type 316NG SS			Type 304 SS					ANL
Cond., μS·cm⁻¹	SO_4^{2-}, ppb	CrO_4^{2-}, ppb	Other, ppb	304 SS, mV(SHE)	Pt, mV(SHE)	Ratio	Freq., 10^{-2} Hz	Time, s	K_{max}[d], MPa·m$^{1/2}$	ΔK,[e] MPa·m$^{1/2}$	Rate,[f] 10^{-10} m·s^{-1}	K_{max}[d], MPa·m$^{1/2}$	ΔK,[e] MPa·m$^{1/2}$	Rate,[g] 10^{-10} m·s^{-1}	EPR, C·cm^{-2}	Ref. No.	Report No.
0.44	15	50	–	37	107	0.95	8	12	–	–	–	27.9	1.39	0.05	0	58	92/6
0.44	15	50	–	37	107	0.95	8	12	–	–	–	36.2	1.81	0.28	8	58	92/6
0.44	15	50	–	37	107	0.95	8	12	–	–	–	30.1	1.50	0.11	30	58	92/6
1.70	100	200	–	108	142	0.95	8	12	–	–	–	27.9	1.39	0.05	0	58	92/6
1.70	100	200	–	108	142	0.95	8	12	–	–	–	37.9	1.89	3.00	8	58	92/6
1.70	100	200	–	108	142	0.95	8	12	–	–	–	30.7	1.53	1.70	30	58	92/6
1.32	50	200	–	14	39	0.95	8	12	–	–	–	27.9	1.39	0.05	0	58	92/6
1.32	50	200	–	14	39	0.95	8	12	–	–	–	38.2	1.91	0.18	8	58	92/6
1.32	50	200	–	14	39	0.95	8	12	–	–	–	30.9	1.54	0.18	30	58	92/6

[a]Compact tension specimens (1TCT) of Type 316NG SS (Heat No. P91576) and Type 304 SS (Heat No. 30956) with the following heat treatments: solution anneal at 1050°C for 0.5 h plus 650°C for 24 h for the Type 316NG SS (EPR = 0 C·cm^{-2}), and solution anneal at 1050°C for 0.5 h (EPR = 0 C·cm^{-2}) followed by 700°C for 0.25 h plus 500°C for 24 h (EPR = 2 C·cm^{-2}), 700°C for 0.67 h (EPR = 8 C·cm^{-2}), 700°C for 12 h (EPR = 20 C·cm^{-2}), or 700°C for 24 h (EPR = 30 C·cm^{-2}) for the Type 304 SS.

[b]Effluent dissolved-oxygen concentration was 200–300 ppb; feedwater oxygen concentration was approximately a factor of 2 higher to compensate for oxygen depletion by corrosion of the autoclave systems.

[c]Positive sawtooth waveform was used.

[d]Stress intensity, K_{max}, values at the end of a ≈1000-h time period of steady-state crack growth.

[e]$\Delta K = K_{max}(1 - R)$, where the load ratio $R = K_{min}/K_{max}$.

[f]Cracking was transgranular, i.e., TGSCC.

[g]Cracking was intergranular, i.e., IGSCC.

[h]Compact tension specimens (0.7TCT) of Type 316NG SS (Heat No. D440104) with the following heat treatment: solution anneal at 1050°C for 0.5 h plus 650°C for 24 h (EPR = 3 C·cm^{-2}).

[i]Sine waveform was used.

Table 11. Summary of Crack Growth Results for Type 347 SS Specimens[a] in Oxygenated Water at 289°C in Which Load Ratio[b] and Stress Intensity Were Varied

Water Chemistry			Potentials		Load		Rise	CGR Data				ANL
Cond.,	O_2,	SO_4^{2-},	304 SS,	Pt,	Ratio	Freq.,	Time,	K_{max}[c],	ΔK,[d]	Rate,	Ref.	Report
$\mu S\ cm^{-1}$	ppb	ppb	mV(SHE)			10^{-2} Hz	s	MPa $m^{1/2}$		10^{-10} m s^{-1}	No.	No.
Slow-Cooled Specimen												
0.92	200	100	147	200	0.90	8	12	19.9	1.99	0.85	62	90/48
0.92	200	100	121	159	0.90	8	12	22.3	2.23	3.40	62	90/48
0.95	200	100	174	223	0.95	8	12	22.4	1.12	0.09	62	90/48
0.96	200	100	185	211	0.95	8	12	27.6	1.38	1.70	62	90/48
0.92	200	100	176	210	0.95	8	12	30.7	1.53	3.00	62	90/48
0.89	200	100	138	174	1.00	0	∞	31.1	0	0.89	62	90/48
Water-Quenched Specimen												
0.93	200	100	150	208	0.50	8	12	19.8	9.90	30.0	62	90/48
0.92	200	100	147	200	0.90	8	12	19.8	1.98	0.09	62	90/48
0.92	200	100	121	159	0.90	8	12	22.0	2.20	1.30	62	90/48
0.95	200	100	174	223	0.95	8	12	22.1	1.11	0.08	62	90/48
0.96	200	100	185	211	0.95	8	12	27.0	1.35	0.60	62	90/48
0.92	200	100	176	210	0.95	8	12	29.8	1.49	0.60	62	90/48
0.89	200	100	138	174	1.00	0	∞	30.0	0	0.61	62	90/48

[a]Compact-tension specimens (1TCT) were fabricated from Heat No. 46113.

[b]Positive sawtooth waveform was used.

[c]Stress intensity, K_{max}, value at the end of each time period.

[d]$\Delta K = K_{max}(1 - R)$, where the load ratio $R = K_{min}/K_{max}$.

5.2 Summary of Crack Growth Data for Ferritic Steels (W. E. Ruther, T. F. Kassner, and J. Y. Park)

Fracture-mechanics CGR tests have been performed on A533-Gr B steel specimens plated with gold, nickel, or nickel-chromium and on composite specimens of A533-Gr B/Inconel-182/Inconel-600 plated with nickel. Test were also conducted on nonplated specimens of A533-Gr B and A106-Gr B steel. The effects of plating, alloy chemistry (e.g., sulfur and phosphorus levels), dissolved-oxygen content (0.2-30 ppm) in 289°C water, and load ratio on CGRs were examined. Tables 12 and 13 summarize results on homogeneous and composite specimens, respectively. It is evident from the results in these tables that the CGRs vary significantly (by a factor of 100) under nominally the same experimental conditions.

Table 12. Summary of Crack Growth Results for Carbon and Low-Alloy Steel Specimens[a-c] in Oxygenated Water at 289°C in Which Load Ratio[d] and Stress Intensity Were Varied

Water Chemistry			Potentials		Load		Rise	CGR Data				ANL
Cond.,	O_2,	SO_4^{2-},	A533-Gr B,	Pt,	Ratio	Freq.,	Time,	K_{max}[e],	ΔK/	Rate,	Ref.	Report
μS cm^{-1}	ppm	ppb	mV(SHE)			10^{-2} Hz	s	MPa m$^{1/2}$		10^{-10} m s^{-1}	No.	No.
Nonplated Specimens												
A533-Gr B Specimen[a] (No. 02C-04) Containing 0.018% S and 0.012% P												
0.12	0.2	-	-94	33	0.25	8	12	20.9	15.65	38.0	23	90/48
0.13	0.2	-	-63	140	0.50	8	12	36.5	18.25	620.0	23	90/48
0.12	0.2	-	38	122	0.95	8	12	44.0	2.20	35.0	23	90/48
0.14	0.2	-	34	68	0.95	8	12	48.5	2.42	3.9	23	90/48
0.12	0.2	-	47	68	0.95	8	12	48.6	2.43	12.0	23	90/48
0.11	0.2	-	21	63	0.95	8	12	49.2	2.46	19.0	23	90/48
0.11	0.2	-	25	75	0.95	8	12	48.8	2.49	16.0	23	90/48
A533-Gr B Specimen[b] (No. CTW7-03) Containing 0.004% S and 0.005% P												
0.19	0.2	-	-	281	0.20	7.7	12	20.1	16.08	55.0	-	92/30
0.19	0.2	-	-	271	0.20	7.7	12	26.3	21.04	100.0	-	92/30
0.07	0.2	-	-	277	0.20	1.6	60	26.5	21.20	20.0	-	92/30
0.08	0.2	-	154	238	0.20	0.9	100	22.4	17.92	1.1	-	92/30
0.07	0.2	-	183	250	0.20	0.13	750	22.4	17.92	1.5	-	92/30
A106-Gr B Specimen[c] (No. CTJ7-01) Containing 0.014% S and 0.014% P												
0.19	0.2	-	-	281	0.20	7.7	12	19.8	15.84	13.0	-	92/30
0.19	0.2	-	-	271	0.20	7.7	12	28.3	22.64	320.0	-	92/30
0.20	0.2	-	-	274	0.20	1.6	60	29.0	23.20	200.0	-	92/30
0.07	0.2	-	-	268	0.70	1.6	60	30.1	9.03	2.0	-	92/30
0.08	0.2	-	154	238	0.20	0.9	100	25.5	20.40	3.0	-	92/30
0.07	0.2	-	183	250	0.20	0.13	750	25.5	20.40	3.0	-	92/30
Plated Specimens												
A533-Gr B Ni-plated Specimen[a] (No. 02C-05) Containing 0.018% S and 0.012% P												
0.12	0.2	-	-94	33	0.25	8	12	20.8	15.60	38.0	23	90/48
0.13	0.2	-	-63	140	0.50	8	12	37.7	18.85	700.0	23	90/48
0.23	0.2	-	1	83	0.80	8	12	58.2	11.64	300.0	23	90/48
0.17	0.2	-	-34	81	0.90	8	12	59.0	5.90	3.8	23	90/48
A533-Gr B Au-plated Specimen[a] (No. 02C-06) Containing 0.018% S and 0.012% P												
0.12	0.2	-	-94	33	0.25	8	12	22.7	17.00	180.0	23	90/48
0.13	0.2	-	-63	140	0.50	8	12	39.5	19.75	430.0	23	90/48
0.23	0.2	-	1	83	0.80	8	12	50.1	10.00	230.0	23	90/48
0.17	0.2	-	-34	81	0.90	8	12	51.0	5.1	6.0	23	90/48
0.16	0.2	-	-80	-4	0.05	8	12	51.3	2.56	0.24	23	90/48
0.14	0.2	-	1	92	0.9[f]	8	12	51.4	2.57	0.31	23	90/48
0.12	0.2	-	47	97	0.95	8	12	60.1	3.00	0.88	23	90/48
0.12	0.2	-	55	75	0.95	8	12	66.8	3.34	83.0	23	90/48
0.17	0.2	-	26	82	0.95	8	12	69.9	3.49	67.0	23	90/48
A533-Gr B Ni-Cr Plated Specimen[a] (No. 02C-07) Containing 0.018% S and 0.012% P												
0.19	0.2	-	-	281	0.20	7.7	12	25.1	18.48	390.0	-	92/30
0.19	0.2	-	-	271	0.20	7.7	12	41.5	33.20	780.0	-	92/30
0.20	0.2	-	-	274	0.20	1.6	60	46.0	36.80	930.0	-	92/30
0.07	0.2	-	-	283	0.20	1.6	60	49.9	39.92	1300.0	-	92/30
0.07	0.2	-	-	278	0.20	1.6	60	55.3	44.24	1600.0	-	92/30
0.07	0.2	-	-	277	0.20	1.6	60	65.2	52.16	2300.0	-	92/30
0.07	0.2	-	-	268	0.70	1.6	60	91.0	27.30	120.0	-	92/30
0.14	0.2	-	-	296	0.50	7.7	12	60.0	30.00	1.1	-	92/30
0.22	0.2	-	-	294	0.40	7.7	12	61.5	36.90	36.0	-	92/30
0.22	0.2	-	-	294	0.40	7.7	12	62.2	37.32	110.0	-	92/30
0.22	0.2	-	-	292	0.40	7.7	12	63.1	37.86	160.0	-	92/30
0.22	0.2	-	-	289	0.40	7.7	12	64.5	38.70	230.0	-	92/30
0.22	0.2	-	-	292	0.40	7.7	12	68.3	40.98	590.0	-	92/30
0.18	0.2	-	-	292	0.40	7.7	12	79.9	47.94	1500.0	-	92/30

Table 12. Continued

Water Chemistry			Potentials			Load Ratio	Rise Time, s	CGR Data				ANL Report No.
Cond., $\mu S\ cm^{-1}$	O_2, ppm	SO_4^{2-}, ppb	A533-Gr B, mV(SHE)	Pt, mV(SHE)		Freq., 10^{-2} Hz		K_{max}[e], MPa $m^{1/2}$	ΔK[f], MPa $m^{1/2}$	Rate, 10^{-10} m s^{-1}	Ref. No.	
A533-Gr B Ni-Cr Plated Specimens[a] (No. 02C-14) Containing 0.018% S and 0.012% P												
0.08	0.2	-	153	231	0.20	7.7	12	21.3	17.04	52.0	-	92/30
0.08	0.2	-	159	231	0.20	3.9	25	21.4	17.12	54.0	-	92/30
0.08	0.2	-	138	227	0.20	2.0	50	21.6	17.28	36.0	-	92/30
0.08	0.2	-	154	238	0.20	0.9	100	21.8	17.44	29.0	-	92/30
0.08	0.2	-	181	239	0.20	0.5	200	21.9	17.52	27.0	-	92/30
0.09	0.2	-	187	251	0.20	0.3	400	21.9	17.52	21.0	-	92/30
0.07	0.2	-	183	250	0.20	0.13	750	22.0	17.60	8.0	-	92/30
0.08	0.2	-	158	237	0.20	0.07	1500	22.0	17.60	1.3	-	92/30
0.10	0.2	-	146	221	0.20	7.7	12	23.3	17.84	59.0	-	92/30

[a]Compact-tension specimens (1TCT) were fabricated from Heat No. A-1195-1, containing 0.018% S and 0.012% P. Specimens were nonplated or electroplated with either nickel, gold, or nickel-chromium.

[b]Compact-tension specimens (1TCT) were fabricated from Heat No. A5401, containing 0.004% S and 0.005% P.

[c]Compact-tension specimens (1TCT) were fabricated from Heat No. J7201, containing 0.014% S and 0.014% P.

[d]Positive sawtooth waveform was used.

[e]Stress intensity, K_{max}, value at the end of each time period.

[f]$\Delta K = K_{max}(1 - R)$, where the load ratio $R = K_{min}/K_{max}$.

Table 13. Summary of Crack Growth Results for Inconel-182/A533-Gr B Specimens[a] in Oxygenated Water[b] at 289°C in Which Load Ratio[c] and Stress Intensity Were Varied

Water Chemistry			Potentials		Load		Rise	IN 182/A533-Gr B				ANL
Cond., μS cm^{-1}	O_2, ppm	SO_4^{2-}, ppb	304 SS, mV(SHE)	Pt,	Ratio	Freq., 10^{-3} Hz	Time, s	$K_{I,max}$[d], MPa m$^{1/2}$	ΔK,[e]	Rate, 10^{-10} m s^{-1}	Ref No	Report No
								Steady-State CGR Data				
0.11	0.2	-	125	140	0.95	8	12	30.8	1.54	0.13	63	91/5
0.10	0.2	-	130	140	0.95	8	12	35.9	1.80	0.16	63	91/5
0.10	0.2	-	120	140	0.95	8	12	42.3	2.12	0.45	63	91/5
0.13	0.2	-	125	130	0.95	8	12	45.2	2.26	0.18	63	91/5
0.12	0.2	-	120	120	0.95	8	12	55.4	2.77	1.09	63	91/5
0.12	0.2	-	120	120	0.95	8	12	63.3	3.17	0.63	63	91/5
0.11	0.2	-	120	120	0.95	8	12	71.5	3.58	0.39	63	91/5
0.11	0.2	-	130	130	0.95	8	12	90.9	4.55	1.14	63	91/5
								Transient CGR Data				
0.11	0.2	-	125	140	0.95	8	12	30.7	1.54	13.1	63	91/5
0.10	0.2	-	130	140	0.95	8	12	35.0	1.75	6.5	63	91/5
0.10	0.2	-	120	140	0.95	8	12	40.0	2.00	16.0	63	91/5
0.12	0.2	-	120	120	0.95	8	12	50.0	2.50	30.1	63	91/5
0.10	0.2	-	12	120	0.95	8	12	62.6	3.13	37.6	63	91/5
0.11	0.2	-	130	130	0.95	8	12	80.0	4.00	30.4	63	91/5
0.12	0.2	-	130	130	0.95	8	12	102.1	5.10	29.2	63	91/5
								Steady-State CGR Data				
0.16	0.3	-	112	126	0.95	8	12	35.0	1.75	20.0	64	92/6
0.16	0.3	-	112	126	0.95	8	12	37.0	1.85	0.30	64	92/6
0.13	0.3	-	49	82	0.95	8	12	40.0	2.00	0.30	64	92/6
0.15	30	-	260	323	0.95	8	12	49.1	2.46	31.0	64	92/6
0.17	0.4	-	96	137	0.95	8	12	50.5	2.53	0.76	64	92/6
0.15	5.9	-	198	321	0.95	8	12	58.6	2.93	69.0	64	92/6
0.13	6.0	-	183	304	1.00	0	∞	59.0	0	0.25	64	92/6
0.17	30	-	220	232	1.00	0	∞	60.0	0	0.81	64	92/6
0.13	31	-	205	204	0.98	8	12	60.1	1.20	0.38	64	92/6
0.14	28	-	223	218	0.95	8	12	60.2	3.01	0.38	64	92/6
0.14	28	-	220	215	0.80	8	12	62.4	6.24	78.0	64	92/6

[a]Composite compact-tension specimens (1TCT) (Nos. 02C-I and 02C-II) were fabricated from Inconel-600/Inconel-182/A533-Gr B Steel (Heat No. A-1195-1, containing 0.018% S and 0.012% P). Specimens were electroplated with nickel.

[b]Effluent dissolved-oxygen concentrations below 20 ppm were determined with an Orbisphere dissolved oxygen meter; higher values were measured with CHEMetrics[TM] ampules.

[c]Positive sawtooth waveform was used.

[d]Stress intensity, K_{max}, value at the end of each time period.

[e]$\Delta K = K_{max}(1 - R)$, where the load ratio $R = K_{min}/K_{max}$.

6 Summary of Results

6.1 Fatigue of Ferritic Piping and Pressure Vessel Steels

- Existing data in the literature on fatigue of carbon steel in LWR environments have been reviewed. Both temperature and dissolved-oxygen concentration in water have a significant effect on fatigue life. In oxygenated water, fatigue life depends strongly on strain rate. For the same environment and strain range, lives can vary by a factor of 100, depending on strain rate. When data are extrapolated to strain rates characteristic of realistic reactor transients (often $<10^{-6}$ s^{-1}), predicted reductions in fatigue life of are ≈1000 or more. However, the relatively good service experience of carbon steel piping in BWRs indicates that extrapolation to such low strain rates is unrealistic and that the effect of strain rate on fatigue life must saturate at some level, although no such saturation has been observed in laboratory tests conducted to date. Based on fracture-mechanics models and engineering judgment, interim fatigue design curves that are also consistent with available data are being developed.

6.2 Stress Corrosion Cracking of Ferritic Steels

- Additional fracture-mechanics CGR tests have been performed on specimens of A533-Gr B steel (nonplated) and on specimens of A106-Gr B and A533-Gr B plated with nickel-chromium. The effect of frequency on CGRs was determined at a load ratio of 0.2 in high-purity oxygenated (≈200 ppb) water at 289°C. The CGRs of the nickel-chromium-plated A533-Gr B specimen were compared with the values predicted by the crack growth curves proposed for inclusion in Section XI of the ASME Boiler and Pressure Vessel Code. The proposed correlations were nonconservative for rise times of ≈100-1000 s in these experiments.

6.3 Irradiation-Assisted Stress Corrosion Cracking of Type 304 SS

- SSRT tests were conducted on CP-grade Type 304 SS specimens obtained from a BWR control-blade sheath to determine SCC susceptibility in simulated BWR water. SCC susceptibility of the sheath was significantly lower than that of neutron-absorber tubes fabricated from another CP-grade and two HP-grade heats of Type 304 SS used in previous investigations. Grain-boundary segregation of impurities in the CP sheath and CP neutron-absorber tube was comparable, except for an indication of C segregation and a higher level of grain-boundary Cr in the sheath material.

- SCC susceptibility of BWR components fabricated from CP and HP heats of Type 304 SS could not be correlated with grain-boundary segregation of Si, P, or S. The relative SCC susceptibility of the HP and CP absorber tubes and the CP sheath could be correlated with minimum grain-boundary Cr contents determined by an AES depth-profiling technique.

6.4 Crack Growth Data Base for Austenitic and Ferritic Steels

- Crack growth tests have been conducted on fracture-mechanics specimens of Types 304, 316NG, and 347 SS and A106-Gr B and A533-Gr B ferritic steel to characterize environmental, loading, and material conditions that can produce SCC susceptibility in these steels. Data that have been obtained over the past eight years (October 1983 to September 1991) are summarized along with references that contain details of the test methods, composition of the materials, metallographic and fractographic information, and comparisons of the data with predictions based on Section XI of the ASME Code.

Acknowledgments

W. F. Burke, D. R. Perkins, and G. J. Talaber contributed to the experimental effort in this program. This work was conducted in programs titled "Environmentally Assisted Cracking in LWR Systems" and "Materials Studies on Service Aged Components" and sponsored by the Office of Nuclear Regulatory Research, U.S. Nuclear Regulatory Commission, under FIN Numbers A22122 and A22562; Program Managers: Drs. J. Muscara and E. Woolridge.

References

1. M. Higuchi and K. Iida, *Fatigue Strength Correction Factors for Carbon and Low-Alloy Steels in Oxygen-Containing High-Temperature Water*, Nucl. Eng. Des., **129**, 293-306 (1991).

2. D. A. Hale, S. A. Wilson, E. Kiss, and A. J. Gianuzzi, *Low Cycle Fatigue Evaluation of Primary Piping Materials in a BWR Environment*, GEAP-20244 (September 1977).

3. D. A. Hale, S. A. Wilson, J. N. Kass, and E. Kiss, *Low Cycle Fatigue Behavior of Commercial Piping Materials in a BWR Environment*, J. of Eng. Mat. and Tech., **103**, 15-25 (1981).

4. S. Ranganath, J. N. Kass, and J. D. Heald, *Fatigue Behavior of Carbon Steel Components in High-Temperature Water Environments*, in Low-Cycle Fatigue and Life Prediction, ASTM STP 770, C. Amzallag, B. N. Leis, and P. Rabbe, eds., American Society for Testing and Materials, Philadelphia, pp. 436-459 (1982).

5. J. B. Terrell, *Effect of Cyclic Frequency on the Fatigue Life of ASME SA-106-B Piping Steel in PWR Environments*, J. Mater. Eng., **10**, 193-203 (1988).

6. B. A. James, L. D. Paul, and M. T. Mighlin, *Low Cycle Fatigue Crack Initiation in SA-210 A1 Carbon Steel Boiler Tubing in Contaminated Boiler Water*, in Fatigue, Degradation and Fracture, PVP-Vol. 195, W. H. Bamford, C. Becht, S. B. Framatome, J. D. Gilman, L. A. James, and M. Prager, eds., American Society of Mechanical Engineers, New York, pp. 13-19 (1990).

7. N. Nagata, S. Sato, and Y. Katada, *Low Cycle Fatigue Behavior of Low Alloy Steels in High Temperature Pressurized Water*, in Trans. 10th Int. Conf. on Structural Mechanics in Reactor Technology, Volume F, A. H. Hadjian, ed., American Association for Structural Mechanics in Reactor Technology, Anaheim, CA (1989).

8. *Criteria of Section III of the ASME Boiler and Pressure Vessel Code for Nuclear Vessels*, The American Society of Mechanical Engineers, United Engineering Center, New York, Library of Congress Catalog No. 56-3934 (1989).

9. N. E. Dowling, *Crack Growth During Low-Cycle Fatigue of Smooth Axial Specimens*, in Cyclic Stress-Strain and Plastic Deformation Aspects of Fatigue Crack Growth, ASTM STP 637, American Society for Testing and Materials, Philadelphia, pp. 97-121 (1977).

10. E. D. Eason, *EDEAC Status: Analysis Procedures for da/dN and S-N Data*, in Technical Information from Workshop Cyclic Life and Environmental Effects in Nuclear Applications, Vol. 2, Clearwater Beach, FL, Pressure Vessel Research Committee and Welding Research Council (January 20-21, 1992).

11. G. M. Wilkowski, F. Brust, R. Francini, N. Ghadiali, T. Kilinski, P. Krishnaswamy, M. Landow, C. W. Marshall, S. Rahaman, and F. Scott, *Short Cracks in Piping and Piping Welds, Semiannual Report October 1990-March 1991*, NUREG/CR-4599, BMI-2173, Vol. 1, No. 2 (1992).

12. H. Abdel-Raouf, A. Plumtree, and T. H. Topper, *Effects of Temperature and Deformation Rate on Cyclic Strength and Fracture of Low-Carbon Steel*, in Cyclic Stress-Strain Behavior--Analysis, Experimentation, and Failure Prediction, ASTM STP 519, L. F. Coffin and E. Krempl, Symposium Co-chairmen, American Society for Testing and Materials, Philadelphia, pp. 28-57 (1973).

13. V. M. Filatov, A. I. Gromova, V. G. Denisov, and V. G. Vasil'ev, *Corrosion Fatigue Test of Steel in Coolant Water*, Ind. Lab. (USSR) **48**, pp. 385-388 (1982). Translated from Zavodskaya Laboratoriya, **48**, pp. 64-67 (1932).

14. P. D. Hicks and F. P. A. Robinson, *Fatigue Crack Growth Rates in a Pressure Vessel Steel under Various Conditions of Loading and the Environment*, Met. Trans. **17A**, 1837-1849 (1986).

15. *Proc. of the Int. Atomic Energy Agency Specialists' Meeting on Subcritical Crack Growth*, NUREG/CP-0044, MEA-2014, Vols. 1 & 2 (May 1983).

16. *Proc. of the 2nd Int. Atomic Energy Agency Specialists' Meeting on Subcritical Crack Growth*, NUREG/CP-0067, MEA-2040, Vols. 1 & 2 (April 1986).

17. *Proc. of the 3rd Int. Atomic Energy Agency Specialists' Meeting on Subcritical Crack Growth*, NUREG/CP-0112, Vols. 1 & 2 (August 1990).

18. T. A. Prater, W. R. Catlin, and L. F. Coffin, *Surface Crack Growth Behavior of Structural Metals in High Temperature Water Environments*, J. Eng. Mater. Technol. **108**, 2-9 (1986).

19. M. O. Speidel and R. M. Magdowski, *Stress Corrosion Cracking of Nuclear Reactor Pressure Vessel Steel in Water: Crack Initiation versus Crack Growth*, Corrosion 88, Paper No. 283, St. Louis, MO (March 1988).

20. D. A. Hale, *The Effect of BWR Startup Environments on Crack Growth in Structural Alloys*, J. Eng. Mater. Technol. **108**, 44–49 (1986).

21. F. P. Ford and P. L. Andresen, *Stress Corrosion Cracking of Low-Alloy Pressure Vessel Steels in 288°C Water*, in Proc. 3rd Int. Atomic Energy Agency Specialists' Meeting on Subcritical Crack Growth, NUREG/CP-0112, Vol. 1, pp. 37–56 (August 1990).

22. P. M. Scott and D. R. Tice, *Stress Corrosion in Low-Alloy Steels*, Nucl. Eng. Des. **119**, 399–413 (1990).

23. J. Y. Park, in *Environmentally Assisted Cracking in Light Water Reactors: Semiannual Report April—September 1989*, NUREG/CR-4667 Vol. 9, ANL-90/48, pp. 12–17 (March 1991).

24. J. Y. Park, in *Environmentally Assisted Cracking in Light Water Reactors: Semiannual Report April—September 1991*, NUREG/CR-4667 Vol. 13, ANL-92/6, pp. 14–16 (March 1992).

25. W. L. Clark and A. J. Jacobs, *Effect of Radiation Environment on SCC of Austenitic Materials*, in Proc. 1st Int. Symp. Environmental Degradation of Materials in Nuclear Power Systems – Water Reactors, National Association of Corrosion Engineers, Houston, pp. 451–461 (1984).

26. F. Garzarolli, D. Alter, and P. Dewes, *Deformability of Austenitic Stainless Steels and Ni-Base Alloys in the Core of a Boiling and Pressurized Water Reactor*, in Proc. 2nd Int. Symp. Environmental Degradation of Materials in Nuclear Power Systems – Water Reactors, National Association of Corrosion Engineers, Houston, pp. 131–138 (1986).

27. F. Garzarolli, D. Alter, P. Dewes, and J. L. Nelson, *Deformability of Austenitic Stainless Steels and Ni-Base Alloys in the Core of a Boiling and Pressurized Water Reactor*, in Proc. 3rd Int. Symp. Environmental Degradation of Materials in Nuclear Power Systems – Water Reactors, G. J. Theus and J. R. Weeks, eds., The Metallurgical Society, Warrendale, PA, pp. 657–664 (1988).

28. H. Hanninen and I. Aho-Mantila, *Environment-Sensitive Cracking of Reactor Internals*, ibid., pp. 77–92.

29. K. Fukuya, S. Nakahigashi, S. Ozaki, M. Teresawa, and S. Shima, *Grain Boundary Segregation of Impurity Atoms In Irradiated Austenitic Stainless Steels*, ibid., pp. 665–671.

30. A. J. Jacobs, G. P. Wozaldo, X. Nakata, T. Yoshida, and I. Masaoka, *Radiation Effects on the Stress Corrosion and Other Selected Properties of Type-304 and Type-316 Stainless Steels*, ibid., pp. 673–681.

31. E. P. Simonen and R. H. Jones, *Calculated Solute Segregation Kinetics Related to Irradiation Assisted Stress Corrosion Cracking*, ibid., pp. 683–690.

32. A. J. Jacobs, R. E. Clausing, L. Heatherly, and R. M. Kruger, *Irradiation-Assisted Stress Corrosion Cracking and Grain Boundary Segregation in Heat-Treated Type 304 SS*, in Effects of Radiation on Materials: 14th Int. Symp., Vol. 1, ASTM STP 1046, N. H. Packan, R. E. Stoller, and A. S. Kumar, eds., American Society for Testing and Materials, Philadelphia, pp. 424–436 (1989).

33. A. J. Jacobs, R. E. Clausing, M. K. Miller, and C. Shepherd, *Influence of Grain Boundary Composition on the IASCC Susceptibility of Type 348 Stainless Steel*, in Proc. 4th Int. Symp. Environmental Degradation of Materials in Nuclear Power Systems – Water Reactors, National Association of Corrosion Engineers, Houston, pp. 14-21 to 14-45 (1990).

34. C. M. Shepherd and T. M. Williams, *Simulation of Microstructural Aspects of IASCC in Water Reactor Core Components*, ibid., pp. 14-11 to 14-20.

35. P. L. Andresen, F. P. Ford, S. M. Murphy, and J. M. Perks, *State of Knowledge of Radiation Effects on Environmental Cracking in Light Water Reactor Core Meterials*, ibid., pp. 1-83 to 1-121.

36. S. Bruemmer, L. A. Charlot, and E. P. Simonen, *Grain Boundary Chemistry Effects on Irradiation-Assisted Stress Corrosion Cracking*, Corrosion 90, Paper No. 506, Las Vegas, NV (April 1990).

37. W. J. S. Yang, *Precipitation Evolution in Type 316 Stainless Steels Irradiated in EBR-II*, in Radiation-Induced Changes in Microstructure: 13th Int. Symp., ASTM STP 955, F. A. Garner, N. H. Packan, and A. S. Kumar, eds., American Society for Testing and Materials, Philadelphia, pp. 628-646 (1987).

38. A. Strasser, J. Santucci, K. Lindquist, W. Vario, G. Stern, L. Goldstein, and L. Joseph, *Evaluation of Stainless Steel Cladding in LWRs*, EPRI NP-2642, Electric Power Research Institute, Palo Alto, CA (December 1982).

39. H. M. Chung and W. E. Ruther, in *Environmentally Assisted Cracking in Light Water Reactors: Semiannual Report, October 1989-March 1990*, NUREG/CR-4667 Vol. 10, ANL-91/5, pp. 14-17 (March 1991).

40. H. M. Chung and W. E. Ruther, in *Environmentally Assisted Cracking in Light Water Reactors: Semiannual Report, April-September 1990*, NUREG/CR-4667 Vol. 11, ANL-91/9, pp. 16-22 (April 1991).

41. H. M. Chung and W. E. Ruther, in *Environmentally Assisted Cracking in Light Water Reactors: Semiannual Report, October 1990-March 1991*, NUREG/CR-4667 Vol. 12, ANL-91/24, pp. 37-54 (August 1991).

42. H. M. Chung, W. E. Ruther, and A. G. Hins, in *Environmentally Assisted Cracking in Light Water Reactors: Semiannual Report, April-September 1991*, NUREG/CR-4667 Vol. 13, ANL-92/6, pp. 20-36 (March 1992).

43. M. Kodama, S. Nishimura, J. Morisawa, S. Shima, S. Suzuki, and M. Yamamoto, *Effects of Fluence and Dissolved Oxygen on IASCC in Austenitic Stainless Steels*, in Proc. 5th Int. Symp. Environmental Degradation of Materials in Nuclear Power Systems – Water Reactors, American Nuclear Society, La Grange Park, IL, 1992, pp. 948-954.

44. H. M. Chung, W. E. Ruther, J. E. Sanecki, and T. F. Kassner, *Irradiation-Induced Sensitization and Stress Corrosion Cracking of Type 304 Stainless Steel Core-Internal Components*, ibid., pp. 795-805.

45. S. M. Bruemmer, L. A. Charlot, and E. P. Simpson, *Irradiation-Induced Chromium Depletion and Its Influence on Intergranular Stress Corrosion Cracking of Stainless Steels*, ibid., pp. 821-826.

46. J. M. Cookson, R. D. Carter, D. L. Damcott, M. Atzmon, G. S. Was, and P. L. Andresen, *Stress Corrosion Cracking of High Energy Proton-Irradiated Stainless Steels*, Ibid., pp. 806-813.

47. K. Fukuya, K. Nakata, and A. Horie, *An IASCC Study Using High Energy Ion Irradiation*, Ibid., pp. 814-820.

48. W. J. Shack, *An Overview of Environmental Degradation of Materials in Nuclear Power Plant Piping Systems*, in Proc. 3rd Int. Symp. Environmental Degradation of Materials in Nuclear Power Systems - Water Reactors, G. J. Theus and J. R. Weeks, eds., The Metallurgical Society, Warrendale, PA, pp. 55-64 (1988).

49. W. E. Ruther, W. K. Soppet, and T. F. Kassner, in *Materials Science and Technology Division Light-Water-Reactor Safety Research Program: Quarterly Progress Report, October - December 1983*, NUREG/CR-3589 Vol. IV, ANL-83-85 Vol. IV, pp. 75-87 (August 1984).

50. W. E. Ruther, W. K. Soppet, and T. F. Kassner, in *Environmentally Assisted Cracking in Light Water Reactors: Annual Report, October 1983 - September 1984*, NUREG/CR-4287, ANL-85-33, pp. 110-113 (June 1985).

51. W. E. Ruther, W. K. Soppet, J. Y. Park, and T. F. Kassner, in *Environmentally Assisted Cracking in Light Water Reactors: Semiannual Report, April - September 1986*, NUREG/CR-4667 Vol. III, ANL-87-37, pp. 2-7 (September 1987).

52. W. E. Ruther, W. K. Soppet, J. Y. Park, and T. F. Kassner, in *Environmentally Assisted Cracking in Light Water Reactors: Semiannual Report, October 1986 - March 1987*, NUREG/CR-4667 Vol. IV, ANL-87-41, pp. 2-10 (December 1987).

53. W. E. Ruther, W. K. Soppet, J. Y. Park, and T. F. Kassner, in *Environmentally Assisted Cracking in Light Water Reactors: Semiannual Report, April - September 1987*, NUREG/CR-4667 Vol. V, ANL-88-32, pp. 3-9 (February 1989).

54. W. E. Ruther, W. K. Soppet, J. Y. Park, and T. F. Kassner, in *Environmentally Assisted Cracking in Light Water Reactors: Semiannual Report, October 1987 - March 1988*, NUREG/CR-4667 Vol. VI, ANL-89/10, pp. 5-14 (August 1989).

55. W. E. Ruther, W. J. Shack, T. F. Kassner, and W. K. Soppet, in *Environmentally Assisted Cracking in Light Water Reactors: Semiannual Report, April 1988 - September 1988*, NUREG/CR-4667 Vol. 7, ANL-89/40, pp. 3-14 (March 1990).

56. W. E. Ruther, J. Y. Park, T. F. Kassner, and W. K. Soppet, in *Environmentally Assisted Cracking in Light Water Reactors: Semiannual Report, October 1988 - March 1989*, NUREG/CR-4667 Vol. 8, ANL-90/4, pp. 2-15 (June 1990).

57. W. E. Ruther, W. K. Soppet, and T. F. Kassner, in *Environmentally Assisted Cracking in Light Water Reactors: Semiannual Report, October 1990 - March 1991*, NUREG/CR-4667 Vol. 12, ANL-91/24, pp. 22-30 (August 1991).

58. W. E. Ruther, W. K. Soppet, and T. F. Kassner, in *Environmentally Assisted Cracking in Light Water Reactors: Semiannual Report, April – September 1991*, NUREG/CR-4667 Vol. 13, ANL-92/6, pp. 16-19 (March 1992).

59. J. Y. Park and W. J. Shack, in *Light-Water-Reactor Safety Research Programs: Quarterly Progress Report, October – December 1984*, NUREG/CR-3998 Vol. III, ANL-84-60 Vol. III, pp. 7-14 (October 1985).

60. J. Y. Park and W. J. Shack, in *Light-Water-Reactor Safety Research Programs: Quarterly Progress Report, January – March 1585*, NUREG/CR-4490 Vol. I, ANL-85-75 Vol. I, pp. 14-16 and 43-49 (March 1986).

61. W. E. Ruther, W. K. Soppet, J. Y. Park, and T. F. Kassner, in *Materials Science and Technology Division Light-Water-Reactor Safety Research Program: Quarterly Progress Report, April – June 1983*, NUREG/CR-3689 Vol. II, ANL-83-85 Vol. II, pp. 44-48 (June 1984).

62. J. Y. Park and W. J. Shack, in *Environmentally Assisted Cracking in Light Water Reactors: Semiannual Report, April 1989 – September 1989*, NUREG/CR-4667 Vol. 9, ANL-90/48, pp. 3-6 (March 1991).

63. W. E. Ruther, T. F. Kassner, and W. K. Soppet, in *Environmentally Assisted Cracking in Light Water Reactors: Semiannual Report, October 1989 – March 1990*, NUREG/CR-4667 Vol. 10, ANL-91/5, pp. 6-13 (March 1991).

64. W. E. Ruther, T. F. Kassner, and W. K. Soppet, in *Environmentally Assisted Cracking in Light Water Reactors: Semiannual Report, April – September 1991*, NUREG/CR-4667 Vol. 13, ANL-92/6, pp. 10-14 (March 1992).

Distribution for NUREG/CR-4667, Vol. 14 (ANL-92/30)

Internal

W. J. Shack (30)

TIS File (3)

ANL Patent File

ANL Contract File

External

NRC, for distribution per R5 (315)

ANL Libraries (2)

Manager, Chicago Operations Office, DOE

Materials and Components Technology Division Review Committee:

A. Berger, Industrial Quality Inc., Gaithersburg, MD

H. Birnbaum, University of Illinois, Urbana

R. C. Buchanan, University of Illinois, Urbana

M. S. Dresselhaus, Massachusetts Institute of Technology, Cambridge, MA

R. A. Greenkorn, Purdue University, West Lafayette, IN

B. Jones, University of Illinois, Urbana

C.-Y. Li, Cornell University, Ithaca, NY

R. Smith, Electric Power Research Institute, NDE Ctr., Charlotte, NC

P. L. Andresen, General Electric Corporate Research and Development, Schenectady, NY

R. G. Ballinger, Massachusetts Institute of Technology, Cambridge, MA

W. H. Bamford, Structural Materials Engineering, Westinghouse Electric Corp., Pittsburgh

S. M. Bruemmer, Battelle Pacific Northwest Laboratory

J. A. Bonucci, Commonwealth Edison Co., Chicago

G. Cragnolino, Southwest Research Inst., San Antonio, TX

R. M. Crawford, Fluor-Daniel Corp., Chicago

D. Cubicciotti, Electric Power Research Inst., Palo Alto, CA

W. H. Cullen, Materials Engineering Assoc., Inc., Lanham, MD

R. Duncan, Combustion Engineering, Inc., Windsor, CT

M. Fox, APTECH, Tucson, AZ

Y. S. Garud, S. Levy, Inc., Campbell, CA

F. Garzarolli, KWU, Erlangen, Germany

J. M. Gordon, General Electric Co., San Jose, CA

S. J. Green, Electric Power Research Institute, Palo Alto, CA

H. E. Hanninen, Technical Research Centre of Finland, Finland

D. Harrison, USDOE, Germantown, MD

J. Hickling, MPA Stuttgart, Stuttgart, Germany

M. E. Indig, General Electric Co., Pleasanton, CA

H. S. Isaacs, Brookhaven National Laboratory

A. Jacobs, General Electric Co., San Jose, CA

L. James, Bettis Atomic Power Laboratory

R. H. Jones, Battelle Pacific Northwest Laboratory

T. Karlsen, OECD Halden Reactor Project, Halden, Norway

J. N. Kass, Lawrence Livermore National Laboratory

C. Kim, Westinghouse Electric Corp., Pittsburgh

L. Ljungberg, ASEA-ATOM, Vasteras, Sweden

C. D. Lundin, U. Tennessee, Knoxville

D. D. Macdonald, Pennsylvania State University, University Park

T. R. Mager, Westinghouse Electric Corp., Pittsburgh

H. Metha, General Electric Co., San Jose, CA

D. Morgan, Pennsylvania Power and Light Co., Allentown, PA

J. L. Nelson, Electric Power Research Inst., Palo Alto, CA

R. A. Oriani, U. Minnesota, Minneapolis

S. Ranganath, General Electric Co., San Jose, CA

E. J. Rowley, Commonwealth Edison Co., Chicago

P. M. Scott, Framatome, Paris, France

C. Shepherd, AEA Technology-Harwell Labs., Didcot, Oxon, UK

P. G. Shewmon, Ohio State University, Columbus

S. Smialowska, Ohio State University, Columbus

M. O. Speidel, Swiss Federal Institute of Technology, Zurich, Switzerland

D. M. Stevens, Lynchburg Research Center, Babcock & Wilcox Co., Lynchburg, VA

W. A. Van Der Sluys, Research & Development Division, Babcock & Wilcox Co., Alliance, OH

E. Venerus, Knolls Atomic Power Laboratory

J. R. Weeks, Brookhaven National Laboratory

D. Winkel, Teleco Oil Field Services, Meriden, CT

A. W. Zeuthen, Long Island Lighting Co., Wading River, NY

NRC FORM 335 (2-89) NRCM 1102, 3201, 3202

U. S. NUCLEAR REGULATORY COMMISSION

BIBLIOGRAPHIC DATA SHEET

(See instructions on the reverse)

1. REPORT NUMBER *(Assigned by NRC. Add Vol., Supp., Rev., and Addendum Numbers, if any.)*
NUREG/CR-4667, Vol. 14
ANL-92/30

2. TITLE AND SUBTITLE
Environmentally Assisted Cracking in Light Water Reactors
Semiannual Report October 1991—March 1992

3. DATE REPORT PUBLISHED
MONTH: August
YEAR: 1992

4. FIN OR GRANT NUMBER
A2212 & 2256

5. AUTHOR(S)
H. M. Chung, T. F. Kassner, S. Majumdar, J. Y. Park, A. Purohit, W. E. Ruther, J. E. Sanecki, and W. J. Shack

6. TYPE OF REPORT
Technical, Semiannual

7. PERIOD COVERED *(Inclusive Dates)*
October 1991—March 1992

8. PERFORMING ORGANIZATION – NAME AND ADDRESS *(If NRC, provide Division, Office or Region, U.S. Nuclear Regulatory Commission, and mailing address; if contractor, provide name and mailing address.)*
Argonne National Laboratory
9700 South Cass Avenue
Argonne, IL 60439

9. SPONSORING ORGANIZATION – NAME AND ADDRESS *(If NRC, type "Same as above"; if contractor, provide NRC Division, Office or Region, U.S. Nuclear Regulatory Commission, and mailing address.)*
Division of Engineering
Office of Nuclear Regulatory Research
U. S. Nuclear Regulatory Commission
Washington, DC 20555

10. SUPPLEMENTARY NOTES

11. ABSTRACT *(200 words or less)*

This report summarizes work performed by Argonne National Laboratory on fatigue and environmentally assisted cracking in light water reactors during the six months from October 1991 through March 1992. Topics that have been investigated during this period include (1) fatigue and stress corrosion cracking of low-alloy steel used in piping and in steam generator and reactor pressure vessels, (2) radiation-induced segregation and irradiation-assisted SCC of Type 304 SS after accumulation of relatively high fluence, and (3) update of a crack growth data base for austenitic and ferritic steels in high-temperature water. Existing data on fatigue of low-alloy steel in LWR environments have been reviewed. Based on fracture-mechanics models and engineering judgement, interim fatigue design curves are being developed that are consistent with available fatigue-life data. Microchemical and microstructural changes in high- and commercial-purity Type 304 SS specimens from control-blade absorber tubes and a control-blade sheath from operating BWRs were studied by Auger electron spectroscopy and scanning electron microscopy. Slow-strain-rate-tensile tests were conducted on irradiated specimens in air and in simulated BWR water at 289°C. Crack growth data on fracture-mechanics specimens of austenitic and ferritic steels in simulated LWR water developed in this program over the past eight years, are compiled into a data base along with references that contain details of test methods, material compositions, metallographic information, and comparisons of data with predictions of Section XI of the ASME Code.

12. KEY WORDS/DESCRIPTORS *(List words or phrases that will assist researchers in locating this report.)*
Corrosion
Crack Growth
Corrosion Fatigue
Stress Corrosion Cracking
Irradiation-Assisted Stress Corrosion Cracking
Radiation-Induced Segregation
A106-Gr B Steel
A533-Gr B Steel
Types 304, 316NG, and 347 Stainless Steel

13. AVAILABILITY STATEMENT
Unlimited

14. SECURITY CLASSIFICATION
(This Page)
Unclassified
(This Report)
Unclassified

15. NUMBER OF PAGES

16. PRICE

NRC FORM 335 (2-89)

Federal Recycling Program